Cumulants and nonlinear response of high p_T harmonic flow at $\sqrt{s_{NN}} = 5.02$ TeV

Jacquelyn Noronha-Hostler,[1] Barbara Betz,[2] Miklos Gyulassy,[3,4,5] Matthew Luzum,[6]
Jorge Noronha,[6] Israel Portillo,[1] and Claudia Ratti[1]

[1]*Department of Physics, University of Houston, Houston, Texas 77204, USA*
[2]*Helene-Wessel-Strasse 12, 53125 Bonn, Germany*
[3]*Nuclear Science Division, Lawrence Berkeley National Laboratory, Berkeley, California 94720, USA*
[4]*Pupin Lab MS-5202, Department of Physics, Columbia University, New York, New York 10027, USA*
[5]*Institute of Particle Physics, Central China Normal University, Wuhan, China*
[6]*Instituto de Física, Universidade de São Paulo, C.P. 66318, 05315-970 São Paulo, SP, Brazil*

(Received 19 October 2016; published 3 April 2017)

Event-by-event fluctuations caused by quantum mechanical fluctuations in the wave function of colliding nuclei in ultrarelativistic heavy ion collisions were recently shown to be necessary for the simultaneous description of $R_{\rm AA}$ as well as the elliptic and triangular flow harmonics at high p_T in PbPb collisions at the Large Hadron Collider (LHC). In fact, the presence of a finite triangular flow as well as cumulants of the flow harmonic distribution that differ from the mean are only possible when these event-by-event fluctuations are considered. In this paper we combine event-by-event viscous hydrodynamics and jet quenching to make predictions for high p_T $R_{\rm AA}$, $v_2\{2\}$, $v_3\{2\}$, and $v_2\{4\}$ in PbPb collisions at $\sqrt{s_{NN}} = 5.02$ TeV. With an order of magnitude larger statistics we find that high p_T elliptic flow does not scale linearly with the soft elliptical flow, as originally thought, but has deviations from perfectly linear scaling. A new experimental observable, which involves the difference between the ratio of harmonic flow cumulants at high and low p_T, is proposed to investigate the fluctuations of high p_T flow harmonics and measure this nonlinear response. By varying the path length dependence of the energy loss and the viscosity of the evolving medium we find that $R_{AA}(p_T)$ and $v_2\{2\}(p_T)$ strongly depend on the choice for the path length dependence of the energy loss, which can be constrained using the new LHC run 2 data.

DOI: 10.1103/PhysRevC.95.044901

I. INTRODUCTION

In recent years, the cumulants of low p_T azimuthal flow harmonic distributions measured in ultrarelativistic heavy ion collisions have been used to attest to the collective behavior of the quark-gluon plasma (QGP) and its description using event-by-event viscous hydrodynamics (for reviews, see Refs. [1–3]). For PbPb collisions at the Large Hadron Collider (LHC) it was found that there is a clear separation between the 2- and 4-particle elliptic flow cumulants, $v_2\{2\}$ and $v_2\{4\}$, respectively, followed by an approximate convergence of higher-order cumulants, i.e., $v_2\{2\} > v_2\{4\} \approx v_2\{6\} \approx v_2\{8\}$ [4–6]. In pPb collisions, where the system formed is considerably smaller, the same behavior for the multiparticle flow cumulants is observed [5,7]. Also, quite strikingly, a similar pattern involving the cumulants of soft anisotropic flow coefficients appears in high multiplicity events in pp collisions at the LHC [8,9], though in this case $v_2\{4\}$ is closer to $v_2\{2\}$ than it is in larger systems [9].

A significant body of research has been developed for studying how initial state fluctuations translate into the final flow harmonics at low p_T. Small-scale subnucleon fluctuations were found to have negligible effect on the lowest-order flow harmonics [10], whereas some sensitivity can be found for subleading modes [11]. In fact, the global shape of the initial condition dominates the description of the flow harmonics at low p_T. For elliptical and triangular flows, v_2 and v_3, respectively, there is a primarily linear mapping between the eccentricity of the initial state ε_2, ε_3 and the final v_2, v_3, i.e., $v_2 \sim \varepsilon_2$ and $v_3 \sim \varepsilon_3$ when the QGP is modeled as a nearly perfect fluid [12–17] (nonlinear corrections only become relevant in this case for peripheral collisions [18,19]). On the other hand, higher-order flow harmonics exhibit nonlinear response via mode mixing [13–17]. Additionally, deviations between higher-order cumulants at low p_T may be attributed to the skewness of the initial eccentricity fluctuations [20,21].

Overall, the mapping between initial state fluctuations and the final flow harmonics in the soft sector has been very successful to the point that event-by-event viscous hydrodynamics [22,23] was able to accurately predict an increase on the order of a few percent in the flow harmonics at LHC when the collision energy was raised from $\sqrt{s_{NN}} = 2.76$ TeV to $\sqrt{s_{NN}} = 5.02$ TeV [24]. This gives support to the current understanding that the initial spatial anisotropies generated by quantum fluctuations in the wave function of the incident nuclei, when combined with event-by-event hydrodynamic simulations for the strongly coupled nearly perfect QGP fluid, can account for the experimentally observed pattern of low p_T azimuthal flow harmonics.

Meanwhile, theoretical understanding of the connection between initial state fluctuations and the experimentally observed flow harmonics at high p_T is still in its infancy. The tomographic aspects of the standard jet quenching-related observables, the nuclear suppression factor R_{AA}, and its azimuthal Fourier components, make them in principle sensitive to the details of the many aspects of our current multilayered description of the bulk QGP evolution, such as: the choice for the initial conditions, the dimensionality of the hydrodynamical evolution (i.e., 2+1 or full 3+1 hydrodynamic simulations), the temperature dependence of the transport coefficients [25–30] and its connection with the

QGP equation of state [31,32], the later stages of hadronic evolution after freeze-out, etc. A systematic study of the many phenomenological parameters currently involved in the hydrodynamic description of the QGP at low p_T can be found in Ref. [33].

An investigation of the influence of these many factors on observables in the hard sector can be carried out by coupling jet tomography models with full event-by-event viscous hydrodynamics, as done for the first time in Ref. [34]. There, it was pointed out that the calculation of high p_T azimuthal coefficients, which are experimentally defined via a nontrivial correlation between soft and hard particles over many events, necessarily requires the use of event-by-event hydrodynamics. In fact, by including the hydrodynamic evolution [35,36] of the initial stage energy density fluctuations in the soft sector and its influence in the hard sector using a simplified jet energy loss model [37–39], a simultaneous description of high p_T R_{AA}, $v_2\{2\}$, and $v_3\{2\}$[1] at LHC $\sqrt{s_{NN}} = 2.76$ TeV was obtained for the first time in Ref. [34]. A further test of this is to make predictions for the R_{AA} and flow harmonics across different collision energies, centralities, and other types of collisions (e.g., pPb).

In this paper, predictions are made for $v_2\{2\}(p_T > 10\,\text{GeV})$, $v_2\{4\}(p_T > 10\,\text{GeV})$, and $v_3\{2\}(p_T > 10\,\text{GeV})$ at LHC $\sqrt{s_{NN}} = 5.02$ TeV for PbPb collisions using event-by-event relativistic hydrodynamics (modeled via the v-USPhydro code [35,36]) and jet tomography (the BBMG model [37–39]). Special care is taken in the theoretical evaluation of these quantities to reproduce the technical procedures used in the experiment, such as the multiplicity weighing process involved in the calculation of the cumulants. We investigate the sensitivity of these observables to the choice of the path length dependence of the energy loss, i.e., $dE/dL \sim L$ or $dE/dL \sim L^2$, the shear viscosity to entropy density ratio, η/s, of the hydrodynamic background, and the jet decoupling parameter (a value of the temperature in the hadronic phase below which energy loss is assumed to vanish). We find that the path length dependence of the energy loss plays a significant role in the calculation of R_{AA} and multiparticle cumulants of high p_T elliptic flow for all centralities while viscosity becomes more relevant in peripheral collisions. On the other hand, we find that viscosity contributes to the decorrelation of soft versus hard event plane angles. Future LHC PbPb run 2 data at $\sqrt{s_{NN}} = 5.02$ TeV will be crucial to determine which type of energy loss model is preferred.

A novel theoretical feature about high p_T anisotropic flow uncovered in this work concerns the *approximate* linear relationship between the event-by-event evaluated soft and hard v_2's discussed in Ref. [34]. A careful analysis involving an order of magnitude more events than used in Ref. [34] reveals that the high p_T v_2^{hard} does not scale perfectly linearly with its soft sector counterpart, v_2^{soft}, but rather has some nonlinear scaling that produces novel results in the cumulants. This deviation from linear response stems from the tomographic nature of the jet energy loss calculations and produces, as a direct consequence, a different value for the $v_2\{4\}(p_T)/v_2\{2\}(p_T)$ ratio in the hard sector in comparison to the corresponding quantity at low p_T. The confirmation of this nonlinear effect could be readily verified using high p_T elliptic flow cumulants from LHC PbPb run 2 data.

This paper is organized as follows. In the next section we give the details about our jet+viscous hydrodynamics model. In Sec. III we discuss the importance of event-by-event fluctuations at high p_T and define the hard sector observables computed in this paper. The dependence of elliptic flow at high p_T with the initial state energy density eccentricities is presented in Sec. IV. Predictions for LHC PbPb data at $\sqrt{s_{NN}} = 5.02$ TeV are shown in Sec. V. A study about the correlation between the event planes in the soft and the hard sectors is done in Sec. VI. We finish with our conclusions and outlook in Sec. VII.

II. COMBINING EVENT-BY-EVENT HYDRODYNAMICS WITH JET TOMOGRAPHY

In this paper we use the same jet energy loss + event-by-event viscous hydrodynamic setup employed in Ref. [34], now to investigate the case of PbPb collisions at $\sqrt{s_{NN}} = 5.02$ TeV. Viscous hydrodynamics is used to model the soft sector on an event-by-event basis and describe the flow harmonics at low p_T. The hydrodynamic fields for each event are then used in the jet energy loss model, which determines the nuclear modification factor and the properties of the flow harmonics in the hard sector event-by-event. The specific details of our model can be found below.

A. Hydrodynamic model

The hydrodynamic evolution of the QGP is modeled through event-by-event simulations performed using the 2+1 (i.e., boost invariant) viscous relativistic hydrodynamics v-USPhydro [35,36]. The equations of motion of viscous hydrodynamics, presented in Ref. [36], are solved using a Lagrangian algorithm called smoothed particle hydrodynamics [41,42]. The accuracy of the code has been demonstrated in Ref. [36] via a comparison to analytical and semianalytical radially expanding solutions of second-order conformal hydrodynamics derived in Ref. [43].

The current version of v-USPhydro contains the leading terms in both the bulk and shear viscosity sectors, which define four transport coefficients: the shear viscosity η and its relaxation time τ_π as well as the bulk viscosity ζ and its corresponding relaxation time τ_Π. As in Ref. [34], in our event-by-event simulations we set η/s to be a constant and neglect effects from bulk viscosity. Effects from additional conserved currents, such as baryon number, are not taken into account.

The initial time of hydrodynamic simulations, τ_0, was set to be $\tau_0 = 0.6$ fm (the initial shear stress tensor, $\pi^{\mu\nu}(\tau_0, x, y)$, is set to zero). We employed the lattice-based equation of state EOS S95n-v1 of Ref. [44] and an isothermal Cooper-Frye [45] freezeout with freeze-out temperature $T_F = 120$ MeV. In v-USPhydro, particle decays are included (with hadronic resonances with masses up to 1.7 GeV) using an adapted version of the corresponding subroutine in the AZHYDRO

[1]Note that $v_3\{2\}$ arises only in the presence of event-by-event fluctuations [40].

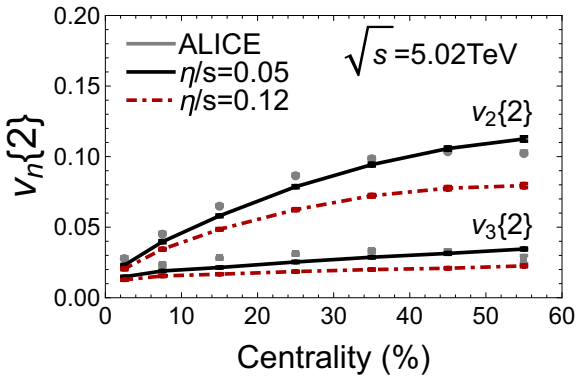

FIG. 1. Model calculations for the soft sector $v_2\{2\}$ and $v_3\{2\}$ as a function of centrality for $0.2 \leqslant p_T \leqslant 3$ GeV, computed using $\eta/s = 0.05$ (black curves) and $\eta/s = 0.12$ (red curves), and their comparison to ALICE $\sqrt{s_{NN}} = 5.02$ TeV PbPb data [24].

code [46]. In this work, we use MCKLN initial conditions [47] for the hydrodynamic simulations (see Ref. [23] for details about these initial conditions at $\sqrt{s_{NN}} = 5.02$ TeV).

At the highest LHC energy the long time spent in the hydrodynamically expanding system is a predominant component in the increase of flow harmonics in the soft sector between LHC run 1 and run 2. As shown in Ref. [23], the change in eccentricities relevant for elliptic flow is only a $\Delta\varepsilon_2 \sim \pm 1\%$ effect. However, holding the eccentricities constant but allowing for a longer hydrodynamical expansion, in order to obtain a 20% increase in the particle distribution, can generate as much as 6% increase in v_2 for the most peripheral collisions (central collisions were found to be largely insensitive to this effect).

We show in Fig. 1 a comparison between our model calculations[2] for the centrality dependence of the p_T-integrated 2-particle cumulants of elliptic and triangular flow, $v_2\{2\}$ and $v_3\{2\}$, and the corresponding ALICE PbPb data at $\sqrt{s_{NN}} = 5.02$ TeV [24]. In this plot, we used 1000 hydrodynamic events per centrality bin. A reasonable agreement with the data is found for $\eta/s = 0.05$, while for $\eta/s = 0.12$ the viscous suppression of the flow harmonics is not compatible with the data.

Such a small value of η/s is a consequence of using MCKLN initial conditions at these higher energies. In fact, at $\sqrt{s_{NN}} = 5.02$ TeV one finds that MCKLN shows a 2–3% decrease in ε_3, while ε_2 is roughly constant [23]. However, ALICE measures a 4.3% increase in triangular flow [24] so if we use the same $\eta/s = 0.11$ as done for run 1 data in Ref. [34], the low p_T flow harmonics are too strongly suppressed. To compensate for this effect, here η/s is decreased to 0.05 to describe $\sqrt{s_{NN}} = 5.02$ TeV data. One fortunate outcome of such as a small η/s is that the reduction of sensitivity to (as yet unknown) initial state $\pi^{\mu\nu}(\tau_0,x,y)$ fluctuations. In contrast, with $\eta/s = 0.2$, as for example used in Ref. [22], even small variations around the assumed initial condition for $\pi^{\mu\nu}(\tau_0,x,y)$ could result in excessively large dissipative corrections to the evolution that still need to be checked. Nevertheless, to check the sensitivity of our results with variations in η/s we also considered the value $\eta/s = 0.12$ in our calculations, as shown in Fig. 1.

Additionally, other effects could cause a difference in η/s across energies such as the fact that the original MCKLN fit of $\eta/s = 0.11$ was made to ATLAS data that has a different p_T range than the ALICE data measured here (ATLAS starts $p_T > 0.5$ GeV, whereas ALICE starts with $p_T > 0.2$ GeV). Furthermore, including charm into the equation of state appears to play a role as one continues to probe higher and higher temperatures [48].

We note that though such a small value of $\eta/s = 0.05$ is below the original "viscosity bound" previously suggested in Ref. [49], it is now understood that finite coupling and N_c corrections can give values of η/s that are indeed below $1/4\pi$ in holographic models [50–53]. In fact, 0.05 is close to the bound derived in Ref. [52] for a class of conformal field theories with Gauss-Bonnet gravity dual. Furthermore, a violation of the bound also appears if local spatial isotropy is broken by the presence of a strong magnetic field [54,55].

B. Jet energy loss model

With all the parameters for the soft sector fixed, we now discuss the details of the jet energy loss model used in this work. In the BBMG model [39] the dependence of the energy loss rate with the jet energy E, path length L, temperature T, and energy loss fluctuations ζ_q is characterized by the parameters (a,z,c,q) that appear in the following formula for the energy loss per unit length,

$$\frac{dE}{dL} = -\kappa\, E^a(L)\, L^z\, T^c\, \zeta_q\, \Gamma_{\rm flow}, \tag{1}$$

where κ is the jet-medium coupling [39], $c = 2 + z - a$, and

$$\Gamma_{\rm flow} = \gamma[1 - v\cos(\phi_{\rm jet} - \phi_{\rm flow})] \tag{2}$$

is the flow factor defined using the local flow velocities of the medium $\vec{u} = \gamma\vec{v}$ (where $\gamma = 1/\sqrt{1-\vec{v}^2}$) [56–58]. This term is important since it couples the differences in path length in the medium to the energy loss experienced by the partons. Moreover, in Eq. (2) $\phi_{\rm jet}$ is the angle defined by the propagating jet in the transverse plane while $\phi_{\rm flow}$ is the local azimuthal angle of the medium constructed using the spatial components of the hydrodynamic flow velocity. The κ parameter in the BBMG energy loss model is completely fixed by setting the computed π^0 $R_{AA}(p_T = 10\,\text{GeV}) \approx 0.17$. We note that in our model effects from the viscosity of the medium on the magnitude of the energy loss are highly indirect since they only appear via the temperature and flow velocity dependence of Eq. (1).

Besides the "pQCD-scenario" used in Refs. [34,39], where $(a = 0,z = 1,c = 3,q = 0)$, i.e., $dE/dL \sim L$, here we also investigate the effects of a quadratic path length dependence [59–62], i.e., $dE/dL \sim L^2$, defined by setting $(a = 0,z = 2,c = 4,q = 0)$ in Eq. (1). We will see in Sec. V that both the nuclear modification factor and the flow harmonics

[2]We note that the multiplicity weighing and the centrality class rebinning procedures, described in Sec. III, are taken into account in these calculations.

are sensitive to this choice for the path length dependence of the energy loss.

In our model the partonic jets are distributed according to event-by-event transverse energy density profiles of the medium given by the v-USPhydro code. The jet path $\vec{x}(L) = \vec{x}_0 + \hat{n}(\phi_{\rm jet})L$ from a production point $\vec{x}_0$ is perpendicular to the beam and moves in the transverse plane along the direction defined by $\phi_{\rm jet}$. Parton distributions from LO perturbative QCD calculations [63] are used. Moreover, we assume that the jets do not lose energy at the points in the medium where the local temperature is smaller than a certain energy scale, which we call the jet-medium decoupling parameter, taken to be either 120 or 160 MeV (below these temperatures standard fragmentation takes place). By varying this phenomenological parameter we can assess part of the uncertainties related to the complicated process of hadronization. Also, as in Ref. [34], we use the KKP pion fragmentation functions [64,65] in our calculations at high p_T. For more details about the BBMG model, we refer the reader to Ref. [39].

III. THE IMPORTANCE OF EVENT-BY-EVENT FLUCTUATIONS AT HIGH TRANSVERSE MOMENTUM

Here we discuss how the inclusion of initial state fluctuations, and their subsequent evolution using event-by-event viscous hydrodynamics, affect the theoretical description of the nuclear modification factor and also the flow harmonics at high p_T. This section contains many details about how to properly compute flow harmonics at high p_T in a way that can be meaningfully compared to experimental data. This discussion largely extends the brief summary presented in Ref. [34] by giving explicit expressions for the cumulants of flow harmonics involving soft and hard hadrons while also providing the details about the multiplicity weighing and centrality class rebinning procedures used in experimental analyses at high p_T.

The energy loss experienced by fast-moving partons in the QGP has been studied over the years using the nuclear modification factor

$$R_{AA}(p_T,\phi) = \frac{1}{\mathcal{N}} \frac{dN_{AA}/dp_T d\phi}{dN_{pp}/dp_T}, \tag{3}$$

where dN_{AA}/dp_T is the particle yield (e.g., pions) per event in AA collisions, dN_{pp}/dp_T is the proton-proton yield, ϕ is the azimuthal angle in the plane transverse to the beam direction, and $\mathcal{N}$ is the appropriate normalization factor (for a given AA centrality) defined in terms of the number of binary collisions [66] and the nucleon-nucleon inelastic cross section. We note that the boost invariance assumption made in this work restricts our calculations to the midrapidity region, $y = 0$.

The azimuthally averaged version of the nuclear modification factor [67–70],

$$R_{AA}(p_T) = \frac{1}{2\pi} \int_0^{2\pi} d\phi \, R_{AA}(p_T,\phi), \tag{4}$$

has been found experimentally [71–77] to strongly depend on global properties of heavy ion events such as their centrality (multiplicity). In fact, in the most central AA collisions where the parton density is the largest, $R_{AA}(p_T)$ at high p_T is strongly suppressed in comparison to the corresponding measurement in peripheral events. This provided an experimentally accessible way to constrain the parameters (and the assumptions) involved in the theoretical modeling of jet energy loss in the QGP including the values and temperature dependence[3] of the jet transport coefficient, $\hat{q}/T^3$, as discussed in detail by the JET-collaboration in Ref. [78].

Important additional information about parton energy loss and its path length dependence in the medium can be obtained by studying the azimuthal anisotropy of high p_T hadrons encoded in $R_{AA}(p_T,\phi)$ [83–85]. In fact, while $R_{AA}(p_T)$ can be described by many different models (see Ref. [78]), to obtain a simultaneous description of $R_{AA}(p_T)$ and high p_T elliptic flow data has proven to be considerably more challenging (see Refs. [39,86] for a discussion).

In general, the azimuthal anisotropy of $R_{AA}(p_T,\phi)$ can be studied using its Fourier harmonics, which we call $v_n^{\rm hard}(p_T)$, defined by the series

$$\frac{R_{AA}(p_T,\phi)}{R_{AA}(p_T)} = 1 + 2\sum_{n=1}^{\infty} v_n^{\rm hard}(p_T) \cos\left[n\phi - n\psi_n^{\rm hard}(p_T)\right], \tag{5}$$

where

$$v_n^{\rm hard}(p_T) = \frac{\frac{1}{2\pi}\int_0^{2\pi} d\phi \, \cos\left[n\phi - n\psi_n^{\rm hard}(p_T)\right] R_{AA}(p_T,\phi)}{R_{AA}(p_T)} \tag{6}$$

and

$$\psi_n^{\rm hard}(p_T) = \frac{1}{n}\tan^{-1}\left(\frac{\int_0^{2\pi} d\phi \, \sin(n\phi)\, R_{AA}(p_T,\phi)}{\int_0^{2\pi} d\phi \, \cos(n\phi)\, R_{AA}(p_T,\phi)}\right). \tag{7}$$

Previous works that investigated high p_T azimuthal anisotropy in the light flavor sector, for instance [39,86], performed their calculations using local temperature and flow profiles from a single event-averaged background given by hydrodynamics, while in Ref. [87] a kinetic theory background was used. This assumption regarding the medium evolution is not realistic given our current understanding of the QGP since it neglects the important role played by initial state fluctuations and their dynamical evolution in the calculation of flow harmonics. For instance, an immediate consequence of the inclusion of event-by-event calculations is that the jet transport parameter $\hat{q}/T^3$ possesses a complicated dependence on space and time that will be different for each hydrodynamic event.

Apart from Ref. [34], previous calculations of high p_T flow harmonics did not include event-by-event viscous hydrodynamics and, thus, could only consider elliptic flow since higher harmonics such as triangular flow are identically zero in this case. As a matter of fact, as stressed in Ref. [34], high $p_T > 10$ GeV flow coefficients such as $v_2\{2\}(p_T)$ are experimentally defined in terms of a 2-particle cumulant involving a soft and a hard hadron. This quantity is intrinsically

[3]The analysis in Ref. [78] gives support to the presence of a peak in $\hat{q}/T^3$ near the crossover region, which is in agreement with nonconformal models that include nonperturbative/strong coupling behavior [79–82].

different than the idealized $v_2^{\rm hard}(p_T)$ in Eq. (6) as it contains the information about the jet-medium interactions encoded in the correlation between soft and hard hadrons. Similar expressions for 4-particle cumulants, e.g., $v_2\{4\}(p_T)$, involving three soft particles and one hard particle can also be computed in our framework, as it will be discussed below.

In the notation used in Refs. [14,17], any flow harmonic V_n can be written as a complex number composed of a magnitude v_n and an angle ψ_n, i.e.,

$$V_n = v_n\, e^{in\psi_n}. \tag{8}$$

Such a representation is useful when one wants to write the expressions for the cumulants. In fact, the correlation between the flow harmonic coefficient taken in the integrated p_T ensemble (soft particles in our case), denoted by V_n, with another flow harmonic at a certain (high) p_T, denoted by $V_n(p_T) = v_n(p_T)\, e^{in\psi_n(p_T)}$, can be simply written as

$$\mathrm{Re}\{V_n V_n^*(p_T)\} = v_n v_n(p_T)\cos\{n[\psi_n - \psi_n(p_T)]\}. \tag{9}$$

Assuming the two particles are independent, this is the probability of finding the pair in a certain azimuthal harmonic n.

Due to finite statistics, one must average correlations over an ensemble of events. This is typically done in the following manner:

(i) The events are separated by their multiplicity into 0.5% centrality subbins.
(ii) Within each centrality subbin the individual flow harmonics are calculated using multiplicity weighing in order to improve statistical error bars.
(iii) The 0.5% centrality subbins are then recombined into larger bins, for instance, of 5% or 10% once again using multiplicity weighing.

In general, multiplicity weighing is used because events with larger multiplicity have less statistical uncertainty. As shown in Ref. [88], it is important when including multiplicity weighing to always use small enough centrality bins because, otherwise, the multiplicity weighing can distort the final results especially in cases where ratios of cumulants of different order, such as $v_2\{4\}/v_2\{2\}$, are taken.

Due to statistical limitations, in this study we will only consider 1% centrality bins and we sort by the number of participants, $N_{\rm part}$, given by our MCKLN initial conditions. The averaging over events within the 1% multiplicity centrality bins is done as in Refs. [89,90] using

$$\langle \dots \rangle = \frac{\sum_i^{\rm events} \mathrm{Re}\{\dots\}_i\, W(n_s,n_h;p_T)_i}{\sum_i^{\rm events} W(n_s,n_h;p_T)_i}, \tag{10}$$

where the weight of each event W_i depends on the number of soft correlated particles, n_s, in the experimental observable as well as on the number of hard correlated particles, n_h, at a given p_T. The weight itself is derived from the total multiplicity for integrated observables or the multiplicity within a specific p_T range for differential observables. In the language of soft versus hard physics, for soft particles the total multiplicity M_i is used while for hard particles one can use the value of $R_{AA}(p_T)_i$ at a specific point in p_T. In this way, the weights read

$$W(2,0)_i = M_i(M_i-1), \tag{11}$$
$$W(4,0)_i = M_i(M_i-1)(M_i-2)(M_i-3), \tag{12}$$
$$W(1,1;p_T)_i = M_i R_{AA}(p_T)_i, \tag{13}$$
$$W(3,1;p_T)_i = M_i(M_i-1)(M_i-2)R_{AA}(p_T)_i. \tag{14}$$

After the experimental observable is obtained in the 1% centrality bins then it must be recombined into a larger bin width, once again using multiplicity weighing to recombine the bins.

We calculate the soft-hard flow harmonic cumulants across p_T using this prescription. For this paper we only consider the 2- and 4-particle cumulants:

$$v_n\{2\}(p_T) = \frac{d_n\{2\}(p_T)}{(c_n\{2\})^{1/2}}, \tag{15}$$
$$v_n\{4\}(p_T) = \frac{d_n\{4\}(p_T)}{(-c_n\{4\})^{3/4}}, \tag{16}$$

where

$$d_n\{2\}(p_T) = \frac{\sum_{j=\mathrm{cent_{start}}}^{\mathrm{cent_{end}}} d_{n,j}\{2\}(p_T)\sum_i^{N_{\rm ev}^j} W(1,1;p_T)_i}{\sum_{j=\mathrm{cent_{start}}}^{\mathrm{cent_{end}}}\sum_i^{N_{\rm ev}^j} W(1,1;p_T)_i}, \tag{17}$$

$$c_n\{2\} = \frac{\sum_{j=\mathrm{cent_{start}}}^{\mathrm{cent_{end}}} c_{n,j}\{2\}\sum_i^{N_{\rm ev}^j} W(2,0)_i}{\sum_{j=\mathrm{cent_{start}}}^{\mathrm{cent_{end}}}\sum_i^{N_{\rm ev}^j} W(2,0)_i}, \tag{18}$$

$$d_n\{4\}(p_T) = \frac{\sum_{j=\mathrm{cent_{start}}}^{\mathrm{cent_{end}}} d_{n,j}\{4\}(p_T)\sum_i^{N_{\rm ev}^j} W(3,1;p_T)_i}{\sum_{j=\mathrm{cent_{start}}}^{\mathrm{cent_{end}}}\sum_i^{N_{\rm ev}^j} W(3,1;p_T)_i}, \tag{19}$$

$$c_n\{4\} = \frac{\sum_{j=\mathrm{cent_{start}}}^{\mathrm{cent_{end}}} c_{n,j}\{4\}\sum_i^{N_{\rm ev}^j} W(4,0)_i}{\sum_{j=\mathrm{cent_{start}}}^{\mathrm{cent_{end}}}\sum_i^{N_{\rm ev}^j} W(4,0)_i}. \tag{20}$$

Here the first sum is over all the subbins j, where $\mathrm{cent_{start}}$ is the start of the centrality class and $\mathrm{cent_{end}}$ is the end of the centrality class (so for 20–30%, $\mathrm{cent_{start}} = 20$ and $\mathrm{cent_{start}} = 30$). The second sum is over the number of events within each 1% subbin where $N_{\rm ev}^j$ is the number of events in the subbin j. The method used here is the scalar product method, which allows for an unambiguous comparison between theory and experiment [91] unlike the previously used event plane method [92].

Returning to Eq. (15), one can see that the 2-particle cumulant is defined in terms of $d_n\{2\}$, which itself is written in terms of the quantities $d_{n,j}\{2\}$ that include a soft and a hard particle within the subbin j,

$$d_{n,j}\{2\}(p_T) = \langle V_n V_n^*(p_T)\rangle_j \tag{21}$$
$$= \langle v_n v_n(p_T)\cos(n[\psi_n - \psi_n(p_T)])\rangle_j, \tag{22}$$

where $\langle\dots\rangle$ is defined in Eq. (10). The normalization factor can be computed using that

$$c_{n,j}\{2\} = \langle V_n V_n^*\rangle_j \tag{23}$$
$$= \langle v_n^2\rangle_j. \tag{24}$$

This shows that the denominator of $v_n\{2\}(p_T)$ in Eq. (15) is exactly the second cumulant of the soft sector, i.e., $v_n\{2\}$. Similarly, it follows that if three soft particles are correlated with one hard particle the ensemble of flow harmonics is

$$d_{n,j}\{4\}(p_T) = 2\langle V_n V_n^*\rangle_j \langle V_n V_n^*(p_T)\rangle_j - \langle V_n V_n^* V_n V_n^*(p_T)\rangle_j \tag{25}$$

$$= 2\, c_{n,j}\{2\} d_{n,j}\{2\}(p_T) - \left\langle v_n^2 V_n V_n^*(p_T)\right\rangle_j \tag{26}$$

$$= 2\, c_{n,j}\{2\} d_{n,j}\{2\}(p_T) - \left\langle v_n^3\, v_n(p_T)\cos(n[\psi_n - \psi_n(p_T)])\right\rangle_j. \tag{27}$$

The normalization factor for the 4-particle cumulant in Eqs. (16) is computed using that

$$-c_{n,j}\{4\} = 2\langle V_n V_n^*\rangle_j^2 - \langle V_n V_n^* V_n V_n^*\rangle_j \tag{28}$$

$$= 2(c_{n,j}\{2\})^2 - \left\langle v_n^4\right\rangle_j. \tag{29}$$

One can see that the denominator in the definition of $v_n\{4\}(p_T)$ is the cubic power of the fourth cumulant of the flow harmonic in the soft sector, $(v_n\{4\})^3$, since there are three soft particles in the numerator.

The discussion above makes it clear that consistent comparisons of theoretical calculations of high p_T flow harmonics to experimental data necessarily require the use of techniques and expertise from event-by-event viscous hydrodynamics. The expressions for the soft-hard cumulants of flow harmonics presented here are valid for any type of jet energy loss model used. Our predictions for the nuclear modification factor and the flow harmonic cumulants for PbPb collisions at $\sqrt{s_{NN}} = 5.02$ TeV at the LHC will be shown in the next section.

Finally, we note that while the dynamically evolving medium affects the energy loss experienced by the jets in our model, the back-reaction of this energy lost by the fast parton onto the medium is not taken into account here. This type of probe approximation, commonly used in jet quenching studies, should hold to determine the properties of the flow harmonics at sufficiently high p_T (e.g., $p_T > 10$ GeV). Between the soft physics hydrodynamical regime and the high p_T limit ($3 \lesssim p_T \lesssim 10$ GeV) lies a region where the influence of jets in the space-time evolution of the QGP may be relevant. If part of the energy lost by jets can quickly thermalize and be distributed in the medium in a collective manner, even the bulk anisotropy of the event and their low p_T flow harmonic coefficients may change [93–97]. Flow measurements typically enforce rapidity gaps between measured particles, in order to suppress nonflow effects. This also has the effect of suppressing the effect of back-reaction, which will likely be limited to rapidities near the jet. However, there still could be some effect from an away-side jet, and in measurements without rapidity gaps, such as $v_n\{4\}(p_T)$.

IV. DEVIATIONS FROM LINEAR RESPONSE

While it is by now well established that the low p_T lowest-order harmonic flow coefficients, such as v_2 and v_3, display an approximate linear behavior with the corresponding eccentricities ε_2 and ε_3 on an event-by-event basis for most centrality classes [14–19], whether or not this type of linear response also holds for harmonic flow at high p_T is not known.

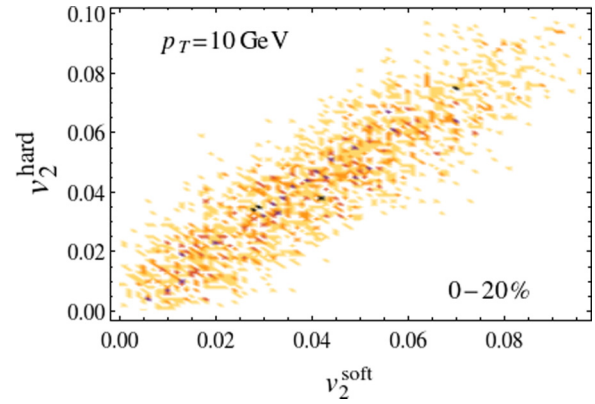

FIG. 2. Event-by-event scatter plot of $v_2^{\rm hard}$ vs. $v_2^{\rm soft}$ at $p_T = 10$ GeV for $\eta/s = 0.05$ in the 0–20% centrality window.

In Ref. [34], a scatter plot of $v_2^{\rm hard}$ [see Eq. (6)], defined in the $20 < p_T < 30$ GeV bin, versus the soft p_T-integrated $v_2^{\rm soft}(0.3 < p_T < 3\,{\rm GeV})$ showed *approximate* linear response behavior for PbPb collisions at $\sqrt{s_{NN}} = 2.76$ TeV. Here we investigate this question regarding linear response of harmonic flow at high p_T using two values of η/s in the soft sector and different p_T cuts in the hard sector. Also, we stress that considerably larger statistics (an order of magnitude more events than in Ref. [34]) are used in the present analysis.

In Figs. 2 and 3 event-by-event scatter plots are shown comparing $v_2^{\rm hard}$ versus $v_2^{\rm soft}$ at $p_T = 10$ GeV for $\eta/s = 0.05$ in 0–20% and 40–60% centrality classes, respectively. Large centrality windows are shown to improve statistics. The approximate, yet imperfect, linear correlation is clearly visible. We note that even at low p_T, flow vectors at different transverse momentum are known not to be perfectly correlated [98]. Thus, it is not surprising to find a similar effect here, where the correlation seems to be even weaker.

We quantify the strength of the correlation by calculating the Pearson correlation coefficient [14,17] between the flow vectors $v_2^{\rm soft}$ and $v_2^{\rm hard}$, and also between $v_2^{\rm hard}$ and ε_2. When the two vectors are perfectly correlated this coefficient goes

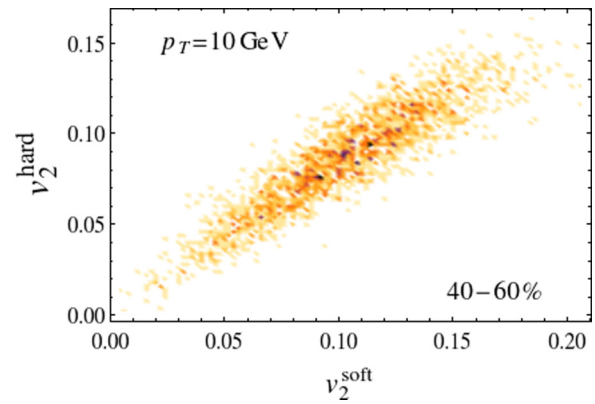

FIG. 3. Event-by-event scatter plot of $v_2^{\rm hard}$ vs. $v_2^{\rm soft}$ at $p_T = 10$ GeV for $\eta/s = 0.05$ in the 40–60% centrality window.

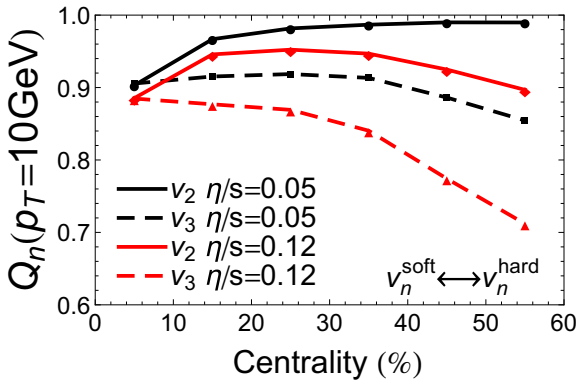

FIG. 4. Pearson Coefficient, Q_n between $v_n^{\rm hard}$ and $v_n^{\rm soft}$, across all centralities, described by Eq. (30) for $p_T = 10$ GeV.

to 1, when they are perfectly anticorrelated it goes to -1, and when there is no linear correlation they go to zero. Here we use the symbol Q_n to describe this linear correlation coefficient between two vectors, such as $v_n^{\rm hard}$ and $v_n^{\rm soft}$ or $v_n^{\rm hard}$ and ε_n. Written in the complex notation (8), this is

$$Q_n(p_T) = \frac{\langle V_n(p_T) V_n^* \rangle}{\sqrt{\langle |V_n(p_T)|^2 \rangle \langle |V_n|^2 \rangle}}. \tag{30}$$

The equivalent expression involving the eccentricity vector is obtained trivially by replacing $V_n \to \varepsilon_n e^{in\Phi_n}$.

One can clearly see that the value of the Pearson coefficient is closest to one when both the magnitude of the flow harmonics and the angles are strongly correlated. If the magnitudes were strongly correlated but the event plane angles were completely decorrelated, or viceversa, then it would still be possible to obtain zero.

The Pearson coefficients for elliptic and triangular flow in Eq. (30) are shown for $p_T = 10$ GeV in Fig. 4 and $p_T = 100$ GeV in Fig. 5 where one can see that a linear correlation between $v_2^{\rm hard}$ and $v_2^{\rm soft}$ is very strong for small values of the viscosity. However, for more central collisions other effects may occur since Q_2 clear deviates from unity and this deviation is correlated with the viscosity (larger viscosity worsens the correlation between $v_2^{\rm hard}$ and $v_2^{\rm soft}$). Thus, we expect elliptic flow at high p_T to display some type of nonlinear response for

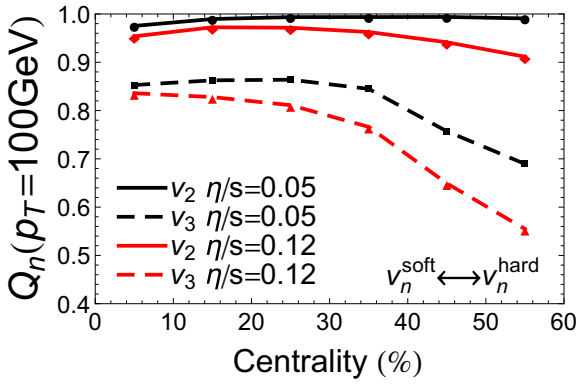

FIG. 5. Pearson coefficient, Q_n between $v_n^{\rm hard}$ and $v_n^{\rm soft}$, across all centralities, described by Eq. (30) for $p_T = 100$ GeV.

most central collisions and that these nonlinearities are tied to viscosity. On the other hand, Fig. 4 shows that the hard and the soft triangular flow are not nearly as strongly correlated. The reason for this is most likely the decorrelation between their event plane angles, as discussed in Sec. VI. Also, we see that there is a significant influence of viscosity on the correlation between hard and soft triangular flow as well. We note that one rather surprising finding is that for central collisions the strength of the correlation is essentially identical for v_2 and v_3 and it may be possible that for super central collisions the linear correlation for v_3 is actually stronger than for v_2.

At higher p_T the linear correlation between $v_2^{\rm hard}$ and $v_2^{\rm soft}$ is considerably improved, especially for central collisions. Furthermore, viscous corrections, while having the same qualitative effect as for $p_T = 10$ GeV, appear to have a smaller influence at high p_T. The correlation of triangular flow worsens at higher p_T, which is likely due to the more decorrelated event plane angles for triangular flow at high p_T seen in Sec. VI.

Finally, we explore the correlation between initial eccentricities and soft flow harmonics. While the soft flow harmonics are already known to be strongly correlated with the initial eccentricities, the linear response is not perfect. Thus, it is not straightforward to see if the eccentricities play a larger role in the formation of $v_n^{\rm hard}$ or if $v_n^{\rm soft}$ is more strongly correlated with $v_n^{\rm hard}$. In Fig. 6 (left plot) we compare the Pearson coefficients between $v_n^{\rm hard}$ and ε_n to the coefficients found using $v_n^{\rm hard}$ and $v_n^{\rm soft}$. As a comparison we also show the very strong correlation between ε_n and $v_n^{\rm soft}$ on the right in Fig. 6.

As expected in the soft physics regime, ε_2 and ε_3 are very strongly correlated with the final $v_2^{\rm soft}$ and $v_3^{\rm soft}$, respectively, in Fig. 6 (right panel). However, the behavior of the flow harmonics in the hard physics region is not so simple. At high p_T the elliptic flow is primarily correlated with the eccentricities, and to a lesser extent with the $v_2^{\rm soft}$. However, triangular flow demonstrates the opposite behavior where $v_3^{\rm soft}$ is a much stronger predictor of $v_3^{\rm hard}$ than the initial eccentricities with the exception of peripheral collisions. This is a rather surprising effect that will be explored in a future study. The effects of the deviation from perfect linear response have an interesting effect on the multiparticle cumulants, especially on the ratio of $v_2\{4\}/v_2\{2\}$, which will be detailed below. In fact, we propose a new variable, $\Delta_n^{\rm SH}$, in the next section that is only nonzero when there are deviations from perfect linear response.

V. PREDICTIONS FOR R_{AA} AND HARMONIC FLOW CUMULANTS AT $\sqrt{s_{NN}} = 5.02$ TeV

In Fig. 7 we show our predictions for π^0 $R_{AA}(p_T)$ for our "standard pQCD-like model" with a linear path length dependence $dE/dL \propto L$, jet-medium decoupling temperature $T_d = 160$ MeV, and $\eta/s = 0.05$ (the value that best describes the soft sector harmonic flow in our model; see Fig. 1). All errors in the plots presented in this paper are statistical and they are calculated with jackknife resampling. Across centralities there is very little change in the p_T dependence of R_{AA} though there is a modest increase around $p_T \sim 10$ GeV as one goes to more peripheral collisions. We checked the dependence of $R_{AA}(p_T)$ with η/s and found that there was no visible

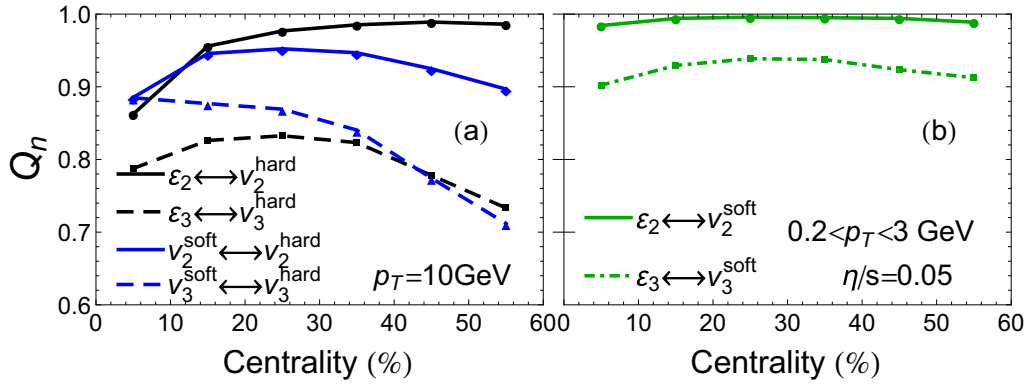

FIG. 6. Pearson coefficient, Q_n between $v_n^{\rm hard}$ and ε_n for $p_T = 100$ GeV (left) and between $v_n^{\rm soft}$ and ε_n (right), across all centralities.

difference between our standard choice of $\eta/s = 0.05$ and the case where $\eta/s = 0.12$ in Fig. 7, thus, $\eta/s = 0.12$ is not shown here.

In Fig. 8 the high p_T 2-particle cumulants of elliptic and triangular flow, $v_2\{2\}(p_T)$ and $v_3\{2\}(p_T)$, are shown across all centralities up to $p_T < 100$ GeV. All the calculations of high p_T cumulants in this paper are for π^0's. Comparisons are shown between the results obtained with two different viscosities, $\eta/s = 0.05$ and $\eta/s = 0.12$, assuming a linear path length dependence for the energy loss $dE/dL \propto L$ and jet-medium decoupling temperature of $T_d = 160$ MeV. The high p_T flow harmonics show essentially no dependence on the viscosity for central to midcentral collisions and they appear to depend on only the initial eccentricities. For peripheral collisions, however, there is some viscosity dependence and, for the most peripheral 50–60% collisions, it may even be possible to exclude one value of the viscosity via a comparison to data (depending on the size of the error bars) assuming that the initial eccentricity is known. That being said, it is clear the viscosity effects in the soft sector, shown in Fig. 1, are at this time more appropriate to constrain the value of this transport coefficient using experimental data. However, for consistency, we expect that the high p_T data would be more compatible with the lowest value of η/s as well.

From Figs. 7 and 8 it appears that $R_{AA}(p_T)$, $v_2\{2\}(p_T)$, and $v_3\{2\}(p_T)$ at $p_T > 10$ GeV have almost no sensitivity to the shear viscosity of the medium. As shown in Ref. [34], as well as in Sec. IV, the eccentricities play the driving role among the bulk parameters in determining the high p_T flow harmonics. In fact, it was shown in Ref. [34] that the high p_T flow harmonics are sensitive to the choice of the initial conditions via its connection with the eccentricities. For instance, one could see in Ref. [34] that the more eccentric MCKLN initial conditions give larger $v_2\{2\}$ at high p_T in comparison to the results found using MCGlauber.

In Fig. 9 we hold the viscosity constant at $\eta/s = 0.05$ and vary either the path length dependence, i.e., $dE/dL \propto L$ versus $dE/dL \propto L^2$ or the jet-medium decoupling temperature $T_d = 160$ MeV versus $T_d = 120$ MeV for the centralities 0–5% and 20–30%. We find no dependence of $R_{AA}(p_T)$ on the jet-medium decoupling temperature. However, there is a clear splitting between the different choices for the path length

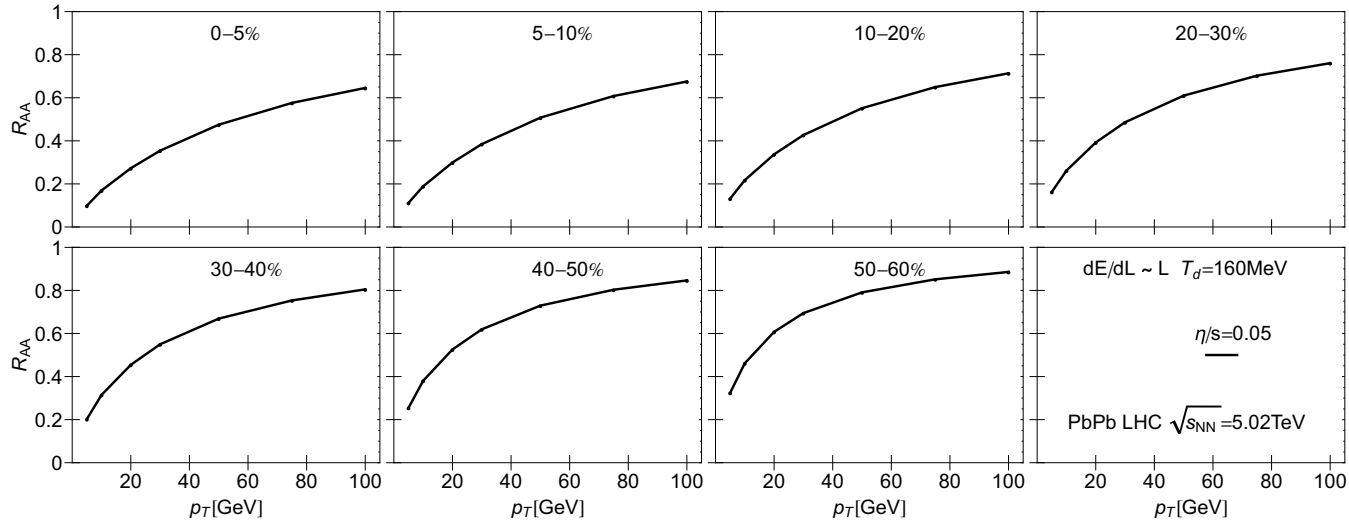

FIG. 7. $R_{AA}(p_T)$ across centralities assuming linear path length dependence of the energy loss $dE/dL \propto L$, jet-medium decoupling temperature $T_d = 160$ MeV, and $\eta/s = 0.05$ across all centralities and plotted up to $p_T = 100$ GeV. All values are calculated for PbPb LHC collisions at $\sqrt{s_{NN}} = 5.02$ TeV.

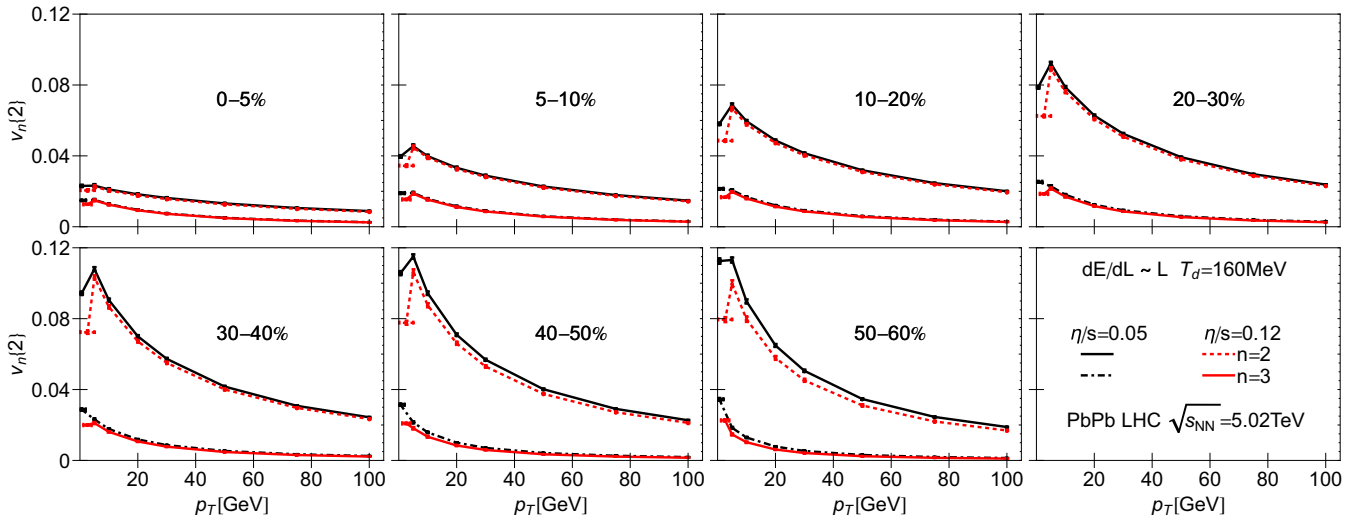

FIG. 8. $v_2\{2\}(p_T)$ and $v_3\{2\}(p_T)$ across centralities computed assuming a linear path length dependence of the energy loss, $dE/dL \propto L$, and jet-medium decoupling temperature $T_d = 160$ MeV. For the black curves $\eta/s = 0.05$ while for the red curves $\eta/s = 0.12$. All values are calculated for PbPb LHC collisions at $\sqrt{s_{NN}} = 5.02$ TeV.

dependence of the energy loss, linear versus quadratic. If the error bars in the future LHC run 2 data are small enough on the 0–5% centrality class it may be possible to exclude one of the possible path length dependencies of the energy loss.

For the flow harmonics there a modest increase in $v_3\{2\}(p_T)$ for the lower decoupling temperature while $v_2\{2\}(p_T)$ actually decreases slightly for 0–5%. Thus, the ratio of $v_2\{2\}(p_T)/v_3\{2\}(p_T)$ is sensitive to the value of T_d though it remains to be seen if that effect is large enough to be constrained by experimental data. While the decoupling temperature has only a modest effect, the path length dependence plays a large role. Both for 0–5% and 20–30% a quadratic path length dependence leads to a significantly larger $v_2\{2\}(p_T)$ and also a larger $v_3\{2\}(p_T)$. Therefore, between $R_{AA}(p_T)$, $v_2\{2\}(p_T)$,

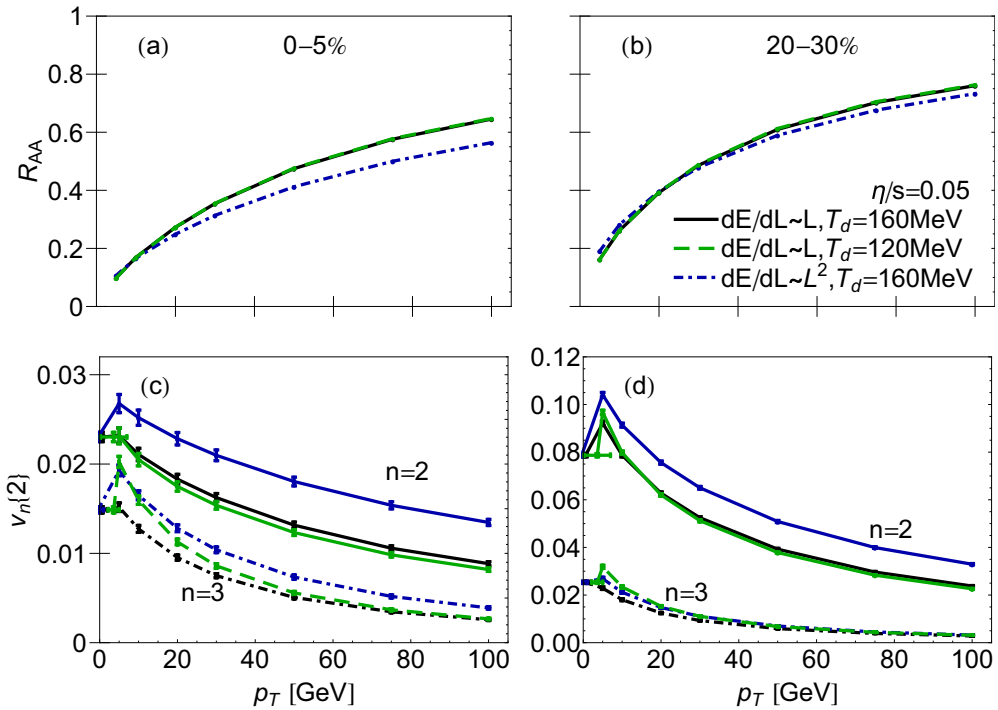

FIG. 9. Variation of $R_{AA}(p_T)$, $v_2\{2\}(p_T)$, and $v_3\{2\}(p_T)$ with the path length dependence $dE/dL \propto L$ vs. $dE/dL \propto L^2$ and the jet-medium decoupling temperature $T_d = 160$ MeV vs. $T_d = 120$ MeV, keeping $\eta/s = 0.05$. Only 0–5% and 20–30% centralities are shown. All values are calculated for PbPb LHC collisions at $\sqrt{s_{NN}} = 5.02$ TeV.

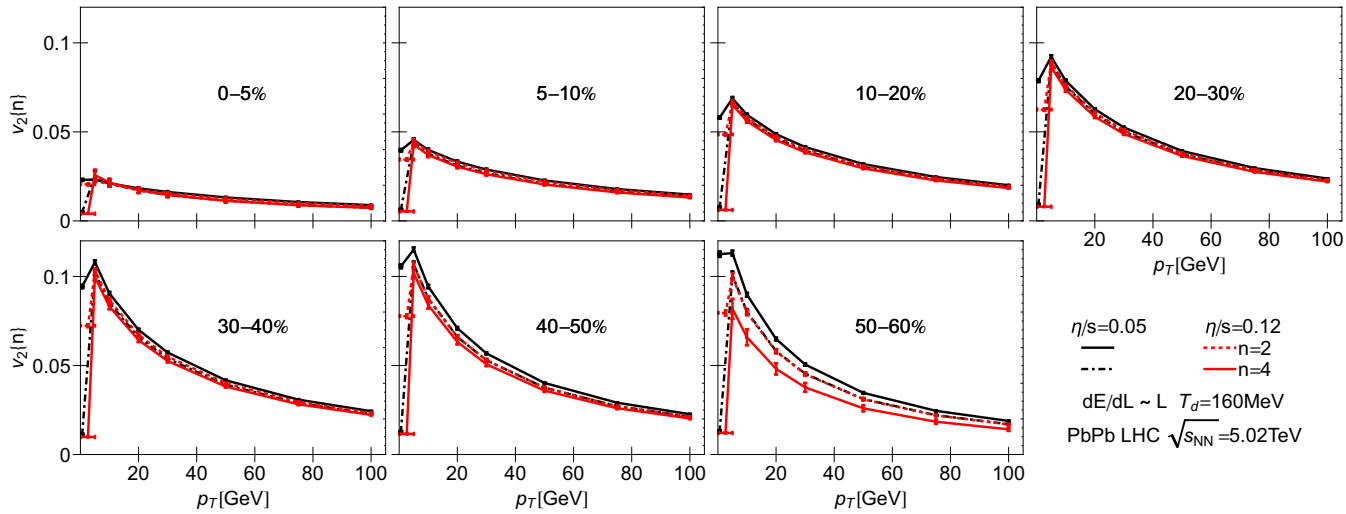

FIG. 10. Cumulants $v_2\{2\}(p_T)$ and $v_2\{4\}(p_T)$ for $\eta/s = 0.05$ and $\eta/s = 0.12$ assuming a linear path length dependence $dE/dL \propto L$ and jet-medium decoupling temperature $T_d = 160$ MeV across centralities. All values are calculated for PbPb LHC collisions at $\sqrt{s_{NN}} = 5.02$ TeV.

and $v_3\{2\}(p_T)$ we expect it to be possible to further constrain the path length dependence of energy loss using the new LHC run 2 data.

In Fig. 10 the results for $v_2\{2\}(p_T)$ and $v_2\{4\}(p_T)$ are shown for $\eta/s = 0.05$ and $\eta/s = 0.12$, assuming a linear path length dependence and $T_d = 160$ MeV across centralities. As in Fig. 8, the effect of viscosity only appears in peripheral collisions. Additionally, we find that the difference between $v_2\{2\}(p_T)$ and $v_2\{4\}(p_T)$ is smaller at high p_T than at low p_T. In order to investigate this effect further the ratio of $v_2\{4\}(p_T)/v_2\{2\}(p_T)$ is shown in Figs. 11–13.

In the low momentum region the ratio $v_2\{4\}/v_2\{2\}$ is often used to judge the strength of the fluctuations (large $v_2\{4\}/v_2\{2\}$ indicates a narrower distribution whereas a smaller value indicates a wider distribution). Specifically, $v_2\{4\}/v_2\{2\}$ is related to the variance of v_n^2, $\sigma^2(v_n^2) \equiv \langle v_2^4\rangle - \langle v_2^2\rangle^2$, as

$$\left(\frac{v_2\{4\}}{v_2\{2\}}\right)^4 = 2 - \frac{\langle v_2^4\rangle}{\langle v_2^2\rangle^2} \tag{31}$$

$$= 1 - \frac{\sigma^2(v_n^2)}{\langle v_2^2\rangle^2}. \tag{32}$$

The differential ratio $v_2\{4\}(p_T)/v_2\{2\}(p_T)$ involves a non-trivial correlation between v_2 at high and low p_T, and is therefore more complicated, as discussed in the next section. However, if there is a perfect linear correlation between the integrated v_2 in each event and $v_2(p_T)$ at a fixed transverse momentum, the ratios are equal.

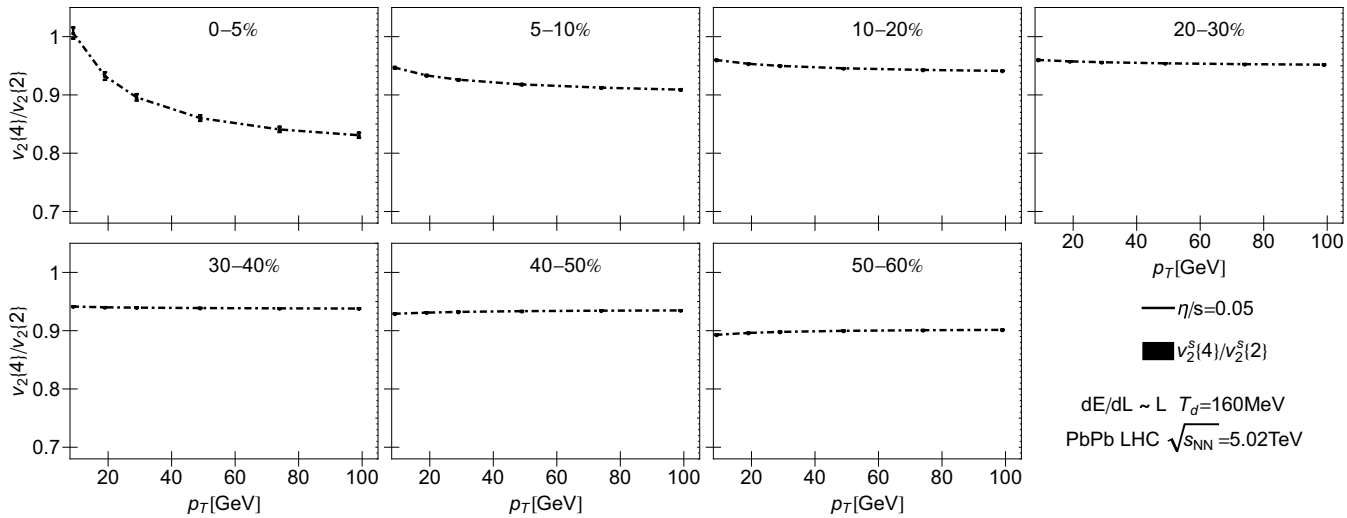

FIG. 11. $v_2\{4\}(p_T)/v_2\{2\}(p_T)$ ratio across centralities for $\eta/s = 0.05$, $dE/dL \propto L$, and jet-medium decoupling parameter $T_d = 160$ MeV. The black band denotes the corresponding value of this ratio in the soft sector. All values are calculated for PbPb LHC collisions at $\sqrt{s_{NN}} = 5.02$ TeV.

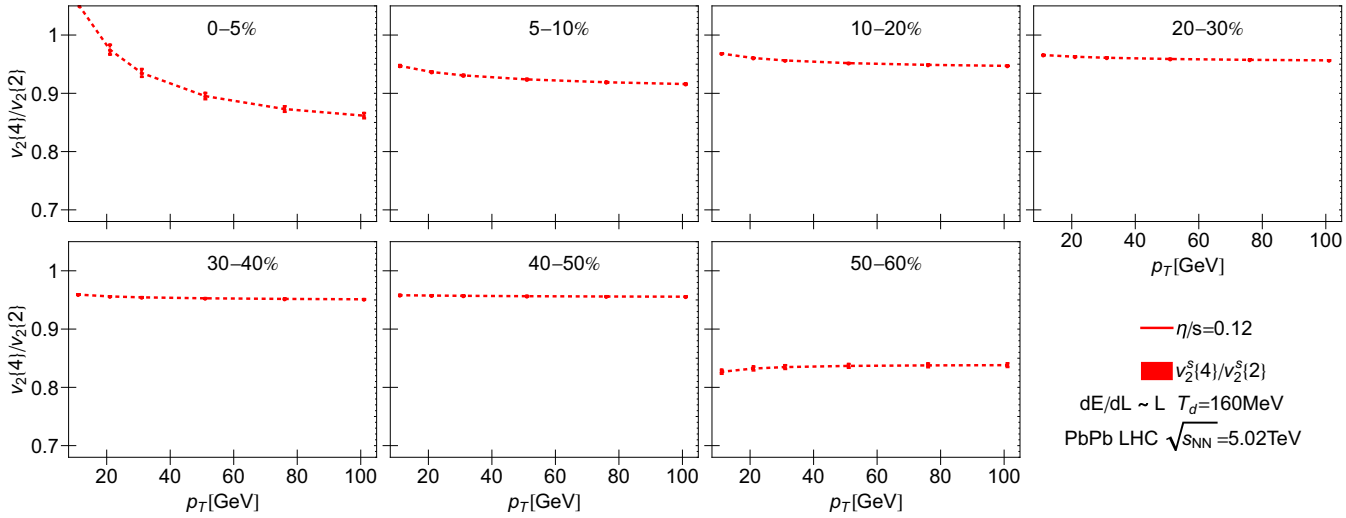

FIG. 12. $v_2\{4\}(p_T)/v_2\{2\}(p_T)$ ratio across centralities for $\eta/s = 0.12$, $dE/dL \propto L$, and jet-medium decoupling parameter $T_d = 160$ MeV. The red band denotes the corresponding value of this ratio in the soft sector. All values are calculated for PbPb LHC collisions at $\sqrt{s_{NN}} = 5.02$ TeV.

Thus, in Fig. 11 we plot the ratio across p_T using our standard scenario with a linear path length dependence, $T_d = 160$ MeV, and $\eta/s = 0.05$. One can see that there is a strong p_T dependence in $v_2\{4\}(p_T)/v_2\{2\}(p_T)$ that approaches unity at $p_T \sim 10$ GeV for central collisions. As one goes toward more peripheral collisions this ratio becomes approximately constant with p_T. The black band is our corresponding prediction for the ratio $v_2\{4\}/v_2\{2\}$ in the soft sector, which is found to be smaller than the differential ratio $v_2\{4\}(p_T)/v_2\{2\}(p_T)$ at high p_T.

As a comparison, in Fig. 12 we increase the viscosity to $\eta/s = 0.12$, keeping the same path length dependence and decoupling temperature as in Fig. 11 to see what effect it has on $v_2\{4\}(p_T)/v_2\{2\}(p_T)$. One can see that the difference between the soft and hard ratios is more pronounced for the larger value of η/s across all centralities. This is consistent with the results shown in Fig. 1.

Finally, in Fig. 13 a direct comparison is shown for different scenarios in the 0–5% centrality bin, which has the largest deviation from the soft sector and the strongest p_T dependence. One can see that a larger viscosity gives the largest $v_2\{4\}(p_T)/v_2\{2\}(p_T)$ ratio and that this is the dominant effect. Changing the path length dependence from $dE/dL \propto L$ to $dE/dL \propto L^2$ has almost no effect on the ratio, which is interesting because this choice has a large effect on $R_{AA}(p_T)$, $v_2\{2\}(p_T)$, and $v_3\{2\}(p_T)$. In fact, looking at $v_2\{4\}(p_T)/v_2\{2\}(p_T)$ provides a method of checking the viscosity fit separately from the path length dependence. Finally, lowering the decoupling temperature to $T_d = 120$ MeV gives a different dependence across p_T for this ratio, which could not be clearly seen in previous plots. Thus, in our model the $v_2\{4\}(p_T)/v_2\{2\}(p_T)$ ratio not only provides interesting information about the fluctuations at high p_T but it also may be used to constrain the medium parameters.

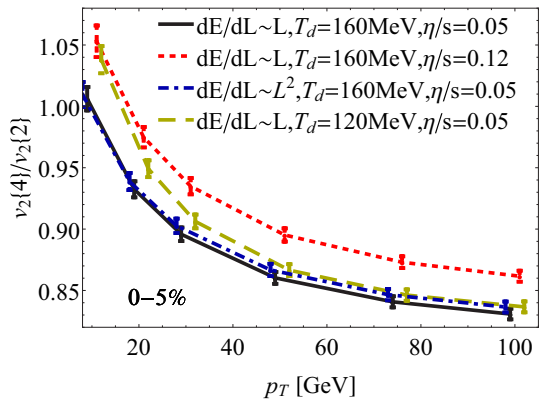

FIG. 13. Variation in the $v_2\{4\}(p_T)/v_2\{2\}(p_T)$ ratio with changes in the path length dependence $dE/dL \propto L$ vs. $dE/dL \propto L^2$ as well as in the jet-medium decoupling temperature $T_d = 160$ MeV vs. $T_d = 120$ MeV, for $\eta/s = 0.05$ and $\eta/s = 0.12$. Only the 0–5% centrality class is shown. All values are calculated for PbPb LHC collisions at $\sqrt{s_{NN}} = 5.02$ TeV.

A. Flow Fluctuations at high p_T

The ratio of integrated cumulants $v_2\{4\}/v_2\{2\}$ is related to the variance of the v_n^2 distribution [see Eq. (31)], and goes to unity as the fluctuations vanish and the variance goes to zero. The differential cumulants $v_n\{k\}(p_T)$, on the other hand, represent a nontrivial correlation between v_n at different transverse momenta [see Eqs. (21) and (28)]. If there are no fluctuations at all (hard or soft), one again obtains a ratio $v_2\{4\}(p_T)/v_2\{2\}(p_T) \sim 1$. However, the converse is not true—a value of 1, such as that seen in central collisions at lower p_T, does *not* necessarily imply a lack of fluctuations in either the hard or soft sector—and unlike the case for integrated cumulants, a value greater than 1 is possible.

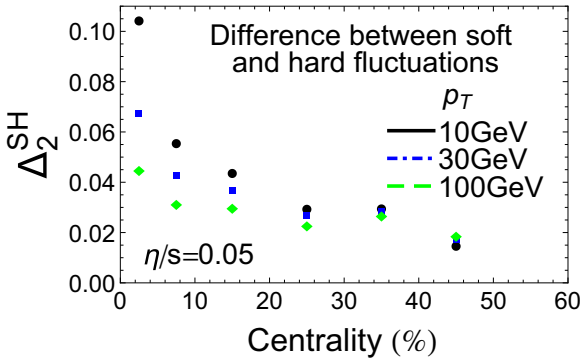

FIG. 14. Difference between the soft and hard fluctuations, $\Delta_2^{\rm SH}$, defined in Eq. (33) for $\eta/s = 0.05$ across all centralities and for three values of p_T.

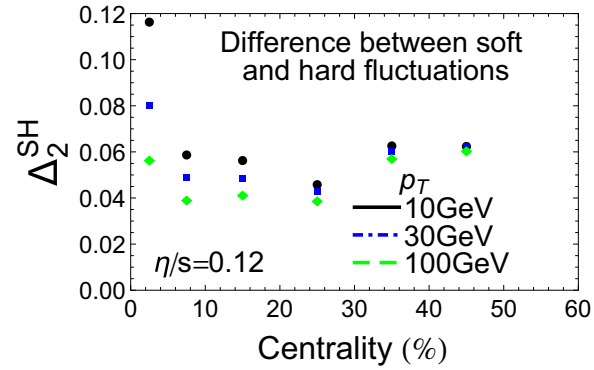

FIG. 15. Difference between the soft and hard fluctuations, $\Delta_2^{\rm SH}$, defined in Eq. (33) for $\eta/s = 0.12$ across all centralities and for three values of p_T.

In fact, flow fluctuations have been well-documented not only in soft physics but also already from experimental data that clear fluctuations in $v_2\{2\}$ have been measured up to p_T 15 GeV [99]. In our model, we can see clear fluctuations in the scatter plot in Fig. 2 despite the fact that the ratio is $v_2\{4\}(p_T)/v_2\{2\}(p_T) \sim 1$ in Fig. 11.

A clearer way to study the difference between harmonic flow fluctuations at low and high p_T may be obtained using the observable

$$\Delta_n^{\rm SH}(p_T) \equiv \underbrace{\frac{\langle v_n^4\rangle}{\langle v_n^2\rangle^2}}_{\text{soft fluctuations}} - \underbrace{\frac{\langle v_n^2 V_n V_n^*(p_T)\rangle}{\langle v_n^2\rangle\langle V_n V_n^*(p_T)\rangle}}_{\text{hard fluctuations}}$$
$$= \underbrace{\left(\frac{v_n\{2\}}{v_n\{4\}}\right)^5\left[\frac{v_n\{4\}(p_T)}{v_n\{2\}(p_T)} - \frac{v_n\{4\}}{v_n\{2\}}\right]}_{\text{Experimental observable}}, \quad (33)$$

where the relationship above is exact (before any centrality rebinning), as shown in the Appendix. If the fluctuations of high p_T elliptic flow were exactly given by the soft fluctuations in a linearly correlated manner (on an event by event basis), i.e., $V_n(p_T) \to \chi_n(p_T)V_n$ with $\chi_n(p_T)$ being the same for all events in the given centrality class, then $\Delta_n^{\rm SH}(p_T)$ would be identically zero for all p_T. The discussion in Sec. IV shows that this should not be the case and, in fact, one can already see in Figs. 11 and 12 that such quantity is nonzero. This implies that Eq. (5) of Ref. [34], which was derived assuming linear response, cannot be used to obtain the correct magnitude of the effects of event-by-event fluctuations on $v_2\{2\}(p_T)$.

In the soft sector, the decorrelation of v_n at different p_T is studied with 2-particle correlations via the factorization breaking ratio r_n [98], or via principle component analysis (PCA) [101]. However, these analyses require a measurement of a 2-particle correlation with both particles at a fixed p_T. For transverse momenta above 10 GeV, this is unfeasible, and it is therefore necessary to study correlations where only 1 of the particles is restricted to a high p_T bin, as we propose here.

Figures 14 and 15 show that $\Delta_2^{\rm SH}(p_T)$ possess a clear dependence on the centrality class and the value of p_T. For the most central collisions and $p_T = 10$ GeV we find the maximum difference between the fluctuations in the soft and hard sectors. As one increases p_T the fluctuations in the soft and hard sectors are more similar (and that is relatively constant across centrality). However, we note that even at very high p_T the assumption of a linear relationship between the high and low p_T elliptic flows does not hold since $\Delta_2^{\rm SH} \neq 0$. Furthermore, a comparison between Figs. 14 and 15 shows that this quantity is also sensitive to the viscosity of the medium. In fact, the difference between the fluctuations in the hard and soft sectors are found to increase with η/s, which is expected given the large sensitivity of the soft flow cumulants with viscosity (see Fig. 1).

VI. SOFT-HARD EVENT PLANE CORRELATION

In Sec. IV the linear relationship between the soft and the hard harmonic flow coefficients was explored in terms of the magnitude of the flow vectors (in the scatter plots of Figs. 2 and 3) and the entire flow vector through linear correlation coefficients Q_n, Eq. (30). One can also visualize how their event plane angle changes at high p_T. As one goes out to higher and higher p_T it is nontrivial to assume that the event plane angle of the integrated soft flow harmonic is correlated with the corresponding quantity at $p_T = 100$ GeV. The correlation function between soft and hard flow harmonics in Eqs. (22) and (27) necessarily contains a cosine term of the difference between their event plane angles. Thus, any degree of decorrelation between these angles decreases the harmonic flow cumulants. In Ref. [100] it was suggested that this decorrelation effect is extremely small for $v_2\{2\}$, whereas $v_3\{2\}$ should be more strongly affected by the decorrelation of the corresponding event plane angles.

Because in this study we have an order of magnitude larger statistics as well as a wider range in parameter variation than Ref. [34], we can determine both how large of an effect the event plane decorrelation has on the flow harmonics and what aspects of the medium influence this decorrelation. In Fig. 16, the difference in the event plane angles at low and high p_T, $P(n[\psi_n^{\rm soft} - \psi_n^{\rm hard}(p_T)])$, at 20–30% centrality is shown for $n = 2$ and $n = 3$. One can clearly see that there is a very strong correlation between the soft and hard angles for elliptic flow, whereas for triangular flow the angles are less correlated, which suppresses $v_3\{2\}(p_T)$. It is also interesting to note that

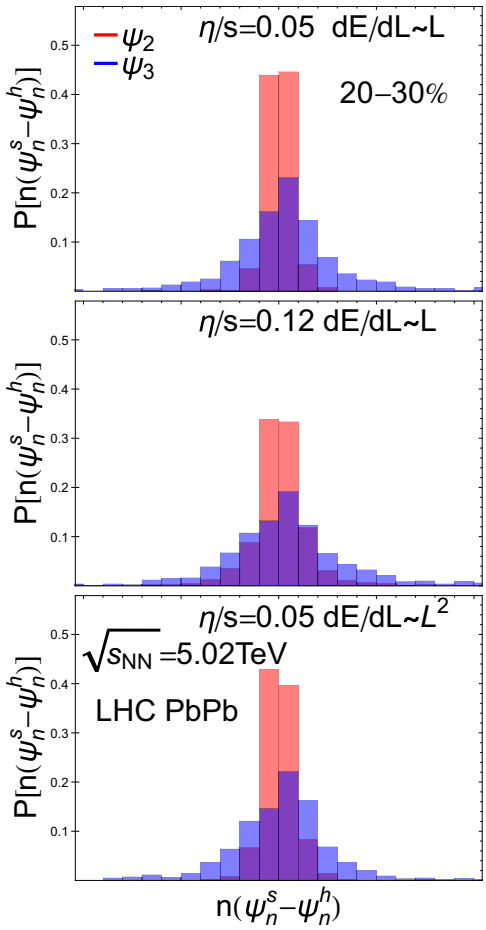

FIG. 16. Distribution of the difference in the event plane angles at low and high p_T, $P(n[\psi_n^{\rm soft} - \psi_n^{\rm hard}(p_T)])$, at 20–30% centrality for LHC PbPb $\sqrt{s_{NN}} = 5.02$ TeV.

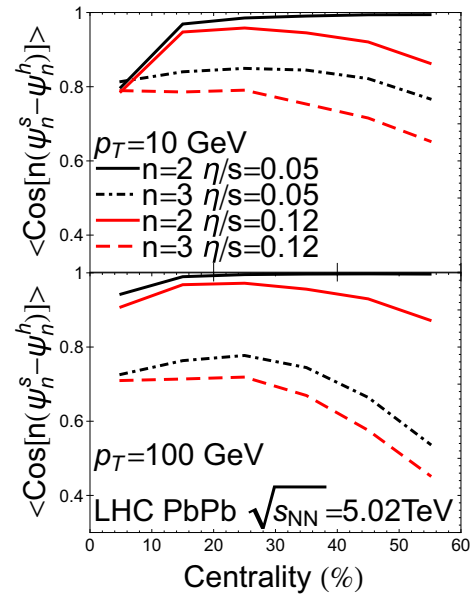

FIG. 17. $\langle \cos n[\psi_n^{\rm soft} - \psi_n^{\rm hard}(p_T)]\rangle$, for $n = 2$ and $n = 3$, across all centralities for two different viscosities $\eta/s = 0.05$ and $\eta/s = 0.12$ for LHC PbPb collisions at $\sqrt{s_{NN}} = 5.02$ TeV.

the path length dependence of the energy loss has essentially no influence on this result, whereas a larger shear viscosity leads to a larger decorrelation in the event plane angles between the soft and the hard sectors.

To see this more clearly we plot in Fig. 17 the mean of the cosine term in the correlation function across centralities, $\langle \cos n[\psi_n^{\rm soft} - \psi_n^{\rm hard}(p_T)]\rangle$. From Fig. 17 one can conclude that the decorrelation of the event plane angles is strongly affected by viscosity. A larger shear viscosity suppresses $\langle \cos n[\psi_n^{\rm soft} - \psi_n^{\rm hard}(p_T)]\rangle$ the most in central and peripheral collisions. The event plane of triangular flow is especially sensitive to this effect. A variation of the path length dependence of the energy loss did not change this result. Thus, our results not only confirm Ref. [100] but we also find that event plane angle decorrelation at high p_T may be used as a probe of the properties of the medium given its strong dependence with viscosity.

VII. CONCLUSIONS AND OUTLOOK

In this paper we used a combination of event-by-event relativistic hydrodynamics, given by the v-USPhydro code, with an energy-loss model, BBMG, to make predictions for the high p_T dependence of $R_{AA}(p_T)$, $v_2\{2\}(p_T)$, $v_3\{2\}(p_T)$, and $v_2\{4\}(p_T)$ of neutral pions in PbPb collisions at $\sqrt{s_{NN}} = 5.02$ TeV, which can be tested against the upcoming results from run 2 data at LHC. Aside from $R_{AA}(p_T)$, none of the 2- and 4-particle cumulants discussed in this paper can be computed without considering the effects of event-by-event viscous hydrodynamics in jet energy loss calculations. In fact, as discussed in Sec. III, in meaningful comparisons to experimental data, the inclusion of event-by-event fluctuations in the theoretical calculation of high p_T flow harmonics is not an option—it is rather mandatory given our current understanding of the bulk evolution of the QGP and the very definition of these observables via event-by-event correlations between soft and hard hadrons. The same reasoning applies to the heavy quark sector (see, e.g., Refs. [102,103] for ideas on how to combine event shape engineering with light and heavy flavor and [104] for the influence of the initial state on heavy flavor flow) and results in this direction will be presented soon. We note that in Refs. [105,106] heavy flavor triangular flow was calculated using the event plane method with an event-by-event ideal hydrodynamic background. In this regard, it would be interesting to study flow harmonic cumulants in the heavy flavor sector following the study done here using event-by-event viscous hydrodynamics.

In order to investigate how our results vary with the assumptions regarding the BBMG energy loss model, we varied the path length dependence of the energy loss, $dE/dL \propto L$ to $dE/dL \propto L^2$. We found a sensitivity of $R_{AA}(p_T)$, $v_2\{2\}(p_T)$, and $v_3\{2\}(p_T)$ with this change. From the combination of the three experimental observables it may be possible to constrain the type of path length dependence of the energy loss using LHC run 2 data. The highest sensitivity occurs for the most central <5% collisions where from Fig. 9 resolving L^1 from

L^2 energy loss will require reduction of systematic errors on both R_{AA} and v_2 to below 0.005. Furthermore, we also tested two different shear viscosities, $\eta/s = 0.05$ and $\eta/s = 0.12$, whose variation has no visible effect on $R_{AA}(p_T)$, though we found that $v_2\{2\}(p_T)$ sees a small suppression for the more peripheral collisions. Overall, the high p_T flow harmonics are found to be much less sensitive to variations of the viscosity than their soft counterparts.

The last parameter that we varied in our study was the jet-medium decoupling temperature, T_d. This phenomenological scale sets the minimum temperature in the hadronic phase, below which energy loss is taken to be zero. In this paper we varied T_d between 120 and 160 MeV and found that most experimental observables appear to be relatively insensitive to T_d, with the exception of the $v_2\{2\}(p_T)$ to $v_3\{2\}(p_T)$ relationship. Triangular flow requires longer system times to build up and, therefore, if the jet is coupled to the medium for a longer period of time then this will enhance $v_3\{2\}(p_T)$.

Here we also investigated the correlation between the soft and the hard event plane angles and its connection to viscosity. We confirm previous results found in Refs. [100] and [34] that the elliptic flow event plane angle at high p_T is strongly correlated to the soft elliptic flow event plane angle. Moreover, we find that an increase in viscosity decorrelates the soft and the hard event plane angles, which is an interesting effect to explore in the future.

Our model allows for the calculation of the difference between the harmonic flow fluctuations in the hard and in the soft sectors, as discussed in detail in Sec. IV. We found that the linear correlation between high p_T elliptic flow and the initial ε_2 is weaker than the correlation between $v_2^{\rm soft}$ and ε_2. Also, triangular flow scales better with $v_3^{\rm soft}$ than with the actual eccentricity ε_3. This deviation from perfect linear scaling of high p_T elliptic flow affects the ratio $v_2\{4\}(p_T)/v_2\{2\}(p_T)$ and experimental verification of this effect can be done through the measurement of the quantity $\Delta_{\rm SH}(p_T)$ defined in Eq. (33), which involves the difference between the soft and hard fluctuations. This quantity depends on the initial conditions and the viscosity of the medium (differently than its soft counterpart) though it does not display a strong sensitivity to the choice for the path length dependence of the energy loss.

In the first attempt of combining event-by-event hydrodynamics with jets [34], the initial conditions were varied and shown to play a significant role in the description of $v_2\{2\}(p_T)$. MCGlauber initial conditions, which have a smaller $\varepsilon_2\{2\}$ than that found in MCKLN initial conditions, consistently were at the low end of the $v_2\{2\}(p_T)$ error bars for LHC Run 1. However, MCKLN initial conditions were found to give a reasonable description of the experimental data at $\sqrt{s_{NN}} = 2.76$ TeV. Due to this result, only MCKLN initial conditions were explored in this study. However, the choice of the initial condition for the hydrodynamic evolution plays a nontrivial role in the study of high p_T flow harmonics and this subject certainly deserves further investigation. Because viscous effects here are small, the initial conditions have a dominant effect at high p_T for $v_2\{2\}$ and $v_3\{2\}$. Thus, high p_T flow harmonic provides a novel (and independent) opportunity to constrain the initial conditions. We hope to see future analyses using Bayesian techniques [33] in viscous hydrodynamics + jet models to determine, in a systematic manner, the allowed range of model parameters that simultaneously describe soft and hard flow harmonics.

Finally, in this paper we went through all the details needed to perform this novel type of theoretical calculations of high p_T flow harmonics event-by-event, including the definition of harmonic flow cumulants at high p_T, which considerably extends the initial study performed in Ref. [34]. Using this knowledge, a similar study could be carried out for hard sector observables using other types of initial conditions, bulk hydrodynamic evolution models (going, for instance, from 2+1 to full 3+1 hydrodynamics) and more realistic energy loss models such as Refs. [82,107–114]. The combination of event-by-event viscous hydrodynamics and jet quenching models is indispensable for calculating triangular flow and multiparticle cumulants of flow harmonics at high p_T. This provides a tool that can be used to understand the correlation between the hard and the soft sectors of heavy ion collisions giving, thus, valuable insight onto how jets interact with the quark-gluon plasma.

ACKNOWLEDGMENTS

The authors thank W. Li, Q. Wang, M. Guilbaud, A. Timmins, A. Suaide, C. Prado, S. Mohapatra, and Y. Zhou for discussions on how to compare theoretical calculations of high p_T harmonic flow to experimental data. We thank X.-N. Wang for providing the LO pQCD parton cross sections. J.N.H. was supported by the National Science Foundation under Grant No. PHY-1513864. J.N.H. and B.B. acknowledge the use of the Maxwell Cluster and the advanced support from the Center of Advanced Computing and Data Systems at the University of Houston to carry out the research presented here. J.N. thanks the University of Houston for its hospitality and Fundação de Amparo à Pesquisa do Estado de São Paulo (FAPESP) and Conselho Nacional de Desenvolvimento Científico e Tecnológico (CNPq) for support.

APPENDIX: DERIVATION OF $\Delta_n^{\rm SH}$

In the following, we will use capital V_n to indicate the vector form of the flow harmonics and the magnitude of a flow harmonic will be written as v_n. In the language of soft versus hard physics, it is understood that a cumulant $v_n\{m\}$ is a soft flow harmonic where as $v_n\{m\}(p_T)$ is the flow harmonic cumulant for the hard sector.

In order to understand the high p_T fluctuations further, we rewrite the ratio $v_2\{4\}(p_T)/v_2\{2\}(p_T)$ using Eqs. (15) and (16) in the simplified vector form (defined in Sec. III), such that

$$\frac{v_n\{4\}(p_T)}{v_n\{2\}(p_T)} = \frac{2\langle V_n V_n^*(p_T)\rangle\langle v_n^2\rangle - \langle v_n^2 V_n V_n^*(p_T)\rangle}{v_n\{4\}^3}\frac{v_n\{2\}}{\langle V_n V_n^*(p_T)\rangle} = \frac{v_n\{4\}}{v_n\{2\}}\left[\frac{2v_n\{2\}^4}{v_n\{4\}^4} - \frac{v_n\{2\}^2}{v_n\{4\}^4}\frac{\langle v_n^2 V_n V_n^*(p_T)\rangle}{\langle V_n V_n^*(p_T)\rangle}\right], \tag{A1}$$

substituting in $2v_n\{2\}^4 = v_n\{4\}^4 + \langle v_n^4\rangle$,

$$\frac{v_n\{4\}(p_T)}{v_n\{2\}(p_T)} = \frac{v_n\{4\}}{v_n\{2\}}\left[1 + \frac{\langle v_n^4\rangle}{v_n\{4\}^4} - \frac{v_n\{2\}^2}{v_n\{4\}^4}\frac{\langle v^2 V V^*(p_T)\rangle}{\langle V V^*(p_T)\rangle}\right] = \frac{v_n\{4\}}{v_n\{2\}}\left[1 + \left(\frac{v_n\{2\}}{v_n\{4\}}\right)^4\left(\frac{\langle v_n^4\rangle}{\langle v_n^2\rangle^2} - \frac{\langle v_n^2 V_n V_n^*(p_T)\rangle}{\langle v_n^2\rangle\langle V_n V_n^*(p_T)\rangle}\right)\right]. \quad \text{(A2)}$$

If the soft and hard flow harmonics fluctuated in the exact same manner then the magnitude of the elliptical flow across all p_T, $|V_n(p_T)|$, would be the magnitude of the integrated elliptical flow $|V_n|$ multiplied with a function that is only depended on p_T: $|V_n(p_T)| \sim \chi_2(p_T)|V_n|$, which means that $\frac{\langle v_n^4\rangle}{\langle v_n^2\rangle^2} - \frac{\langle v_n^2 V_n V_n^*(p_T)\rangle}{\langle v_n^2\rangle\langle V_n V_n^*(p_T)\rangle} \to 0$ and then the ratio $\frac{v_n\{4\}}{v_n\{2\}}(p_T) = \frac{v_n\{4\}}{v_n\{2\}}$ would be constant across p_T.

Thus, the deviation from $\frac{v_n\{4\}}{v_n\{2\}}(p_T) = \frac{v_n\{4\}}{v_n\{2\}}$ in Figs. 11 and 12 implies that the relationship between the integrated elliptical flow is not linear with the differential elliptical flow. Indeed, the correction term to $\frac{v_n\{4\}}{v_n\{2\}}$ in Eq. (A2) returns the exact deviation seen in Figs. 11 and 12 and is typically between 0.02 and 0.06 with the exception of centrality classes in the 0–10% range.

Experimentally, it is possible to determine the difference between the soft and hard fluctuations, which we defined as $\Delta_n^{\rm SH}$ in Eq. (33),

$$\Delta_n^{\rm SH}(p_T) \equiv \underbrace{\frac{\langle v_n^4\rangle}{\langle v_n^2\rangle^2}}_{\text{soft fluctuations}} - \underbrace{\frac{\langle v_n^2 V_n V_n^*(p_T)\rangle}{\langle v_n^2\rangle\langle V_n V_n^*(p_T)\rangle}}_{\text{hard fluctuations}} = \underbrace{\left(\frac{v_n\{2\}}{v_n\{4\}}\right)^5\left[\frac{v_n\{4\}(p_T)}{v_n\{2\}(p_T)} - \frac{v_n\{4\}}{v_n\{2\}}\right]}_{\text{Experimental observable}}, \quad \text{(A3)}$$

where we rearranged Eq. (A2) to obtain the experimental observable. Note that the definition of $\Delta_n^{\rm SH}$ is exact when no multiplicity weighing is used to recombine centrality bins.

[1] U. Heinz and R. Snellings, Annu. Rev. Nucl. Part. Sci. **63**, 123 (2013).
[2] M. Luzum and H. Petersen, J. Phys. G **41**, 063102 (2014).
[3] R. Derradi de Souza, T. Koide, and T. Kodama, Prog. Part. Nucl. Phys. **86**, 35 (2016).
[4] S. Chatrchyan *et al.* (CMS Collaboration), Phys. Rev. C **89**, 044906 (2014).
[5] B. B. Abelev *et al.* (ALICE Collaboration), Phys. Rev. C **90**, 054901 (2014).
[6] G. Aad *et al.* (ATLAS Collaboration), Eur. Phys. J. C **74**, 3157 (2014).
[7] V. Khachatryan *et al.* (CMS Collaboration), Phys. Rev. Lett. **115**, 012301 (2015).
[8] G. Aad *et al.* (ATLAS Collaboration), Phys. Rev. Lett. **116**, 172301 (2016).
[9] V. Khachatryan *et al.* (CMS Collaboration), Phys. Lett. B **765**, 193 (2017).
[10] J. Noronha-Hostler, J. Noronha, and M. Gyulassy, Phys. Rev. C **93**, 024909 (2016).
[11] A. Mazeliauskas and D. Teaney, Phys. Rev. C **93**, 024913 (2016).
[12] D. Teaney and L. Yan, Phys. Rev. C **83**, 064904 (2011).
[13] Z. Qiu and U. W. Heinz, Phys. Rev. C **84**, 024911 (2011).
[14] F. G. Gardim, F. Grassi, M. Luzum, and J. Y. Ollitrault, Phys. Rev. C **85**, 024908 (2012).
[15] D. Teaney and L. Yan, Phys. Rev. C **86**, 044908 (2012).
[16] H. Niemi, G. S. Denicol, H. Holopainen, and P. Huovinen, Phys. Rev. C **87**, 054901 (2013).
[17] F. G. Gardim, J. Noronha-Hostler, M. Luzum, and F. Grassi, Phys. Rev. C **91**, 034902 (2015).
[18] H. Niemi, K. J. Eskola, and R. Paatelainen, Phys. Rev. C **93**, 024907 (2016).
[19] J. Noronha-Hostler, L. Yan, F. G. Gardim, and J. Y. Ollitrault, Phys. Rev. C **93**, 014909 (2016).
[20] H. Grönqvist, J. P. Blaizot, and J. Y. Ollitrault, Phys. Rev. C **94**, 034905 (2016).
[21] G. Giacalone, L. Yan, J. Noronha-Hostler, and J. Y. Ollitrault, Phys. Rev. C **95**, 014913 (2017).
[22] H. Niemi, K. J. Eskola, R. Paatelainen, and K. Tuominen, Phys. Rev. C **93**, 014912 (2016).
[23] J. Noronha-Hostler, M. Luzum, and J. Y. Ollitrault, Phys. Rev. C **93**, 034912 (2016).
[24] J. Adam *et al.* (ALICE Collaboration), Phys. Rev. Lett. **116**, 132302 (2016).
[25] J. Noronha-Hostler, J. Noronha, and C. Greiner, Phys. Rev. Lett. **103**, 172302 (2009).
[26] J. Noronha-Hostler, J. Noronha, and C. Greiner, Phys. Rev. C **86**, 024913 (2012).
[27] G. S. Denicol, H. Niemi, E. Molnar, and D. H. Rischke, Phys. Rev. D **85**, 114047(E) (2012); **91**, 039902(E) (2015).
[28] S. I. Finazzo, R. Rougemont, H. Marrochio, and J. Noronha, J. High Energy Phys. 02 (2015) 051.
[29] R. Rougemont, J. Noronha, and J. Noronha-Hostler, Phys. Rev. Lett. **115**, 202301 (2015).
[30] J. Noronha-Hostler, arXiv:1512.06315 [nucl-th].
[31] S. Borsanyi, Z. Fodor, C. Hoelbling, S. D. Katz, S. Krieg, and K. K. Szabo, Phys. Lett. B **730**, 99 (2014).
[32] A. Bazavov, T. Bhattacharya, C. DeTar, H. T. Ding, S. Gottlieb, R. Gupta, P. Hegde, U. M. Heller, F. Karsch, E. Laermann, L. Levkova, S. Mukherjee, P. Petreczky, C. Schmidt, C. Schroeder, R. A. Soltz, W. Soeldner, R. Sugar, M. Wagner, and P. Vranas, (HotQCD Collaboration), Phys. Rev. D **90**, 094503 (2014).
[33] J. E. Bernhard, J. S. Moreland, S. A. Bass, J. Liu, and U. Heinz, Phys. Rev. C **94**, 024907 (2016).
[34] J. Noronha-Hostler, B. Betz, J. Noronha, and M. Gyulassy, Phys. Rev. Lett. **116**, 252301 (2016).

[35] J. Noronha-Hostler, G. S. Denicol, J. Noronha, R. P. G. Andrade, and F. Grassi, Phys. Rev. C **88**, 044916 (2013).
[36] J. Noronha-Hostler, J. Noronha, and F. Grassi, Phys. Rev. C **90**, 034907 (2014).
[37] B. Betz, M. Gyulassy, and G. Torrieri, Phys. Rev. C **84**, 024913 (2011).
[38] B. Betz and M. Gyulassy, Phys. Rev. C **86**, 024903 (2012).
[39] B. Betz and M. Gyulassy, J. High Energy Phys. 08 (2014) 090; 10 (2014) 043.
[40] B. Alver and G. Roland, Phys. Rev. C **81**, 054905 (2010); **82**, 039903(E) (2010).
[41] L. B. Lucy, Astrophys. J. **82**, 1013 (1977); R. A. Gingold and J. J. Monaghan, Mon. Not. R. Astron. Soc. **181**, 375 (1977); J. J. Monaghan, Annu. Rev. Astron. Astrophys. **30**, 543 (1992); E. Chow and J. J. Monaghan, J. Comput. Phys. **134**, 296 (1997).
[42] C. E. Aguiar, T. Kodama, T. Osada, and Y. Hama, J. Phys. G **27**, 75 (2001).
[43] H. Marrochio, J. Noronha, G. S. Denicol, M. Luzum, S. Jeon, and C. Gale, Phys. Rev. C **91**, 014903 (2015).
[44] P. Huovinen and P. Petreczky, Nucl. Phys. A **837**, 26 (2010).
[45] F. Cooper and G. Frye, Phys. Rev. D **10**, 186 (1974).
[46] P. F. Kolb, J. Sollfrank, and U. Heinz, Phys. Rev. C **62**, 054909 (2000); P. F. Kolb and R. Rapp, *ibid.* **67**, 044903 (2003); P. F. Kolb and U. Heinz, arXiv:nucl-th/0305084.
[47] H.-J. Drescher and Y. Nara, Phys. Rev. C **75**, 034905 (2007).
[48] S. Borsanyi *et al.*, Nature **539**, 69 (2016).
[49] P. K. Kovtun, D. T. Son, and A. O. Starinets, Phys. Rev. Lett. **94**, 111601 (2005).
[50] Y. Kats and P. Petrov, J. High Energy Phys. 01 (2009) 044.
[51] M. Brigante, H. Liu, R. C. Myers, S. Shenker, and S. Yaida, Phys. Rev. D **77**, 126006 (2008).
[52] M. Brigante, H. Liu, R. C. Myers, S. Shenker, and S. Yaida, Phys. Rev. Lett. **100**, 191601 (2008).
[53] A. Buchel, R. C. Myers, and A. Sinha, J. High Energy Phys. 03 (2009) 084.
[54] R. Critelli, S. I. Finazzo, M. Zaniboni, and J. Noronha, Phys. Rev. D **90**, 066006 (2014).
[55] S. I. Finazzo, R. Critelli, R. Rougemont, and J. Noronha, Phys. Rev. D **94**, 054020 (2016).
[56] N. Armesto, C. A. Salgado, and U. A. Wiedemann, Phys. Rev. C **72**, 064910 (2005).
[57] T. Renk and J. Ruppert, Phys. Rev. C **72**, 044901 (2005).
[58] R. Baier, A. H. Mueller, and D. Schiff, Phys. Lett. B **649**, 147 (2007).
[59] C. Marquet and T. Renk, Phys. Lett. B **685**, 270 (2010).
[60] J. Jia, W. A. Horowitz, and J. Liao, Phys. Rev. C **84**, 034904 (2011).
[61] J. Jia and R. Wei, Phys. Rev. C **82**, 024902 (2010).
[62] A. Adare *et al.* (PHENIX Collaboration), Phys. Rev. C **87**, 034911 (2013).
[63] X.-N. Wang (private communication).
[64] B. A. Kniehl, G. Kramer, and B. Potter, Nucl. Phys. B **597**, 337 (2001).
[65] F. Simon (STAR Collaboration), AIP Conf. Proc. **870**, 428 (2006).
[66] M. L. Miller, K. Reygers, S. J. Sanders, and P. Steinberg, Annu. Rev. Nucl. Part. Sci. **57**, 205 (2007).
[67] M. Gyulassy and M. Plumer, Phys. Lett. B **243**, 432 (1990).
[68] X. N. Wang and M. Gyulassy, Phys. Rev. D **44**, 3501 (1991).
[69] X. N. Wang and M. Gyulassy, Phys. Rev. Lett. **68**, 1480 (1992).
[70] I. Vitev and M. Gyulassy, Phys. Rev. Lett. **89**, 252301 (2002).
[71] K. Adcox *et al.* (PHENIX Collaboration), Phys. Rev. Lett. **88**, 022301 (2002).
[72] C. Adler *et al.* (STAR Collaboration), Phys. Rev. Lett. **89**, 202301 (2002).
[73] S. S. Adler *et al.* (PHENIX Collaboration), Phys. Rev. Lett. **91**, 072301 (2003).
[74] J. Adams *et al.* (STAR Collaboration), Phys. Rev. Lett. **91**, 172302 (2003).
[75] J. Adams *et al.* (STAR Collaboration), Phys. Rev. Lett. **91**, 072304 (2003).
[76] B. Abelev *et al.* (ALICE Collaboration), Phys. Lett. B **720**, 52 (2013).
[77] S. Chatrchyan *et al.* (CMS Collaboration), Eur. Phys. J. C **72**, 1945 (2012).
[78] K.M. Burke, A. Buzzatti, N. Chang, C. Gale, M. Gyulassy, U. Heinz, S. Jeon, A. Majumder, B. Muller, G. Y. Qin, B. Schenke, C. Shen, X. N. Wang, J. Xu, C. Young, and H. Zhang (JET Collaboration), Phys. Rev. C **90**, 014909 (2014).
[79] J. Liao and E. Shuryak, Phys. Rev. Lett. **102**, 202302 (2009).
[80] D. Li, J. Liao, and M. Huang, Phys. Rev. D **89**, 126006 (2014).
[81] R. Rougemont, A. Ficnar, S. Finazzo, and J. Noronha, J. High Energy Phys. 04 (2016) 102.
[82] J. Xu, J. Liao, and M. Gyulassy, J. High Energy Phys. 02 (2016) 169.
[83] X. N. Wang, Phys. Rev. C **63**, 054902 (2001).
[84] M. Gyulassy, I. Vitev, and X. N. Wang, Phys. Rev. Lett. **86**, 2537 (2001).
[85] E. V. Shuryak, Phys. Rev. C **66**, 027902 (2002).
[86] J. Xu, J. Liao, and M. Gyulassy, Chin. Phys. Lett. **32**, 092501 (2015).
[87] D. Molnar and D. Sun, arXiv:1305.1046 [nucl-th].
[88] F. G. Gardim, F. Grassi, M. Luzum, and J. Noronha-Hostler, Phys. Rev. C **95**, 034901 (2017).
[89] A. Bilandzic, R. Snellings, and S. Voloshin, Phys. Rev. C **83**, 044913 (2011).
[90] A. Bilandzic, C. H. Christensen, K. Gulbrandsen, A. Hansen, and Y. Zhou, Phys. Rev. C **89**, 064904 (2014).
[91] M. Luzum and J. Y. Ollitrault, Phys. Rev. C **87**, 044907 (2013).
[92] A. M. Poskanzer and S. A. Voloshin, Phys. Rev. C **58**, 1671 (1998).
[93] L. G. Pang, Q. Wang, X. N. Wang, and R. Xu, Phys. Rev. C **81**, 031903 (2010).
[94] Y. Tachibana and T. Hirano, Phys. Rev. C **90**, 021902 (2014).
[95] R. P. G. Andrade, J. Noronha, and G. S. Denicol, Phys. Rev. C **90**, 024914 (2014).
[96] M. Schulc and B. Tomàsik, Phys. Rev. C **90**, 064910 (2014).
[97] L. V. Bravina *et al.*, Eur. Phys. J. C **75**, 588 (2015).
[98] F. G. Gardim, F. Grassi, M. Luzum, and J. Y. Ollitrault, Phys. Rev. C **87**, 031901 (2013).
[99] G. Aad *et al.* (ATLAS Collaboration), Phys. Rev. C **92**, 034903 (2015).
[100] J. Jia, Phys. Rev. C **87**, 061901 (2013).
[101] R. S. Bhalerao, J. Y. Ollitrault, S. Pal, and D. Teaney, Phys. Rev. Lett. **114**, 152301 (2015).
[102] P. Christiansen, J. Phys. Conf. Ser. **736**, 012023 (2016).
[103] C. A. G. Prado, J. Noronha-Hostler, M. R. Cosentino, M. G. Munhoz, J. Noronha, and A. A. P. Suaide, J. Phys. Conf. Ser. **779**, 012035 (2017).

[104] S. Cao, G. Y. Qin, and S. A. Bass, Phys. Rev. C **88**, 044907 (2013).
[105] M. Nahrgang, J. Aichelin, S. Bass, P. B. Gossiaux, and K. Werner, Phys. Rev. C **91**, 014904 (2015).
[106] M. Nahrgang, J. Aichelin, P. B. Gossiaux, and K. Werner, Phys. Rev. C **93**, 044909 (2016).
[107] M. Gyulassy, P. Levai, and I. Vitev, Nucl. Phys. B **594**, 371 (2001).
[108] J. Xu, A. Buzzatti, and M. Gyulassy, J. High Energy Phys. 08 (2014) 063.
[109] X. Guo and X. N. Wang, Phys. Rev. Lett. **85**, 3591 (2000).
[110] X. N. Wang and X. Guo, Nucl. Phys. A **696**, 788 (2001).
[111] A. Majumder, Phys. Rev. D **85**, 014023 (2012).
[112] G. Y. Qin, J. Ruppert, C. Gale, S. Jeon, G. D. Moore, and M. G. Mustafa, Phys. Rev. Lett. **100**, 072301 (2008).
[113] B. Schenke, C. Gale, and S. Jeon, Phys. Rev. C **80**, 054913 (2009).
[114] K. C. Zapp, F. Krauss, and U. A. Wiedemann, J. High Energy Phys. 03 (2013) 080.